Stem Cell Reports
Article

OPEN ACCESS

Scalable Production of iPSC-Derived Human Neurons to Identify Tau-Lowering Compounds by High-Content Screening

Chao Wang,[1,2,7] Michael E. Ward,[1,2,5,7] Robert Chen,[2] Kai Liu,[3,4] Tara E. Tracy,[1,2] Xu Chen,[1,2] Min Xie,[3,4] Peter Dongmin Sohn,[1,2] Connor Ludwig,[2] Anke Meyer-Franke,[1] Celeste M. Karch,[6] Sheng Ding,[3,4] and Li Gan[1,2,*]

[1]Gladstone Institute of Neurological Disease, 1650 Owens Street, San Francisco, CA 94158, USA
[2]Department of Neurology, University of California, San Francisco, 675 Nelson Rising Lane, San Francisco, CA 94158, USA
[3]Gladstone Institute of Cardiovascular Disease, 1650 Owens Street, San Francisco, CA 94158, USA
[4]Department of Pharmaceutical Chemistry, University of California, San Francisco, 600 16th Street, San Francisco, CA 94158, USA
[5]National Institute of Neurological Disorders and Stroke, National Institutes of Health, 35 Convent Drive, Bethesda, MD 20892, USA
[6]Department of Psychiatry, Washington University School of Medicine, 425 South Euclid Avenue, St. Louis, MO 63110, USA
[7]Co-first author
*Correspondence: lgan@gladstone.ucsf.edu
http://dx.doi.org/10.1016/j.stemcr.2017.08.019

SUMMARY

Lowering total tau levels is an attractive therapeutic strategy for Alzheimer's disease and other tauopathies. High-throughput screening in neurons derived from human induced pluripotent stem cells (iPSCs) is a powerful tool to identify tau-targeted therapeutics. However, such screens have been hampered by heterogeneous neuronal production, high cost and low yield, and multi-step differentiation procedures. We engineered an isogenic iPSC line that harbors an inducible neurogenin 2 transgene, a transcription factor that rapidly converts iPSCs to neurons, integrated at the AAVS1 locus. Using a simplified two-step protocol, we differentiated these iPSCs into cortical glutamatergic neurons with minimal well-to-well variability. We developed a robust high-content screening assay to identify tau-lowering compounds in LOPAC and identified adrenergic receptors agonists as a class of compounds that reduce endogenous human tau. These techniques enable the use of human neurons for high-throughput screening of drugs to treat neurodegenerative disease.

INTRODUCTION

The microtubule-associated neuronal protein tau stabilizes microtubules and mediates axon outgrowth and axonal transport. Abnormal tau is strongly implicated in Alzheimer's disease (AD) and other neurodegenerative tauopathies (Wang and Mandelkow, 2016). Although intraneuronal aggregates of insoluble tau fibrils, known as neurofibrillary tangles, are a hallmark of tauopathies and correlate with cognitive decline in AD (Nelson et al., 2012), soluble tau may also play a key pathogenic role (Brunden et al., 2008; Spires-Jones et al., 2011). In *Drosophila* and mouse models, overexpression of wild-type human tau induces neurodegeneration (Wittmann et al., 2001), axonopathy (Spittaels et al., 1999), and extensive cell death (Andorfer et al., 2005) independently of tangle formation. In two regulatable tauopathy mouse models, suppressing soluble tau expression resulted in memory recovery (Santacruz et al., 2005; Sydow et al., 2011) and stabilized neuron numbers (Santacruz et al., 2005) without reducing the level of neurofibrillary tangles, suggesting that soluble forms of tau promote neurodegeneration. Lowering endogenous tau levels reduces amyloid β (Aβ)-induced behavioral deficits in AD mouse models (Roberson et al., 2007; Vossel et al., 2010), and lowering total tau levels by inhibiting tau acetylation or phosphorylation rescues tau-related memory deficits in PS19 transgenic mice (Lasagna-Reeves et al., 2016; Min et al., 2015). Since tau knockout mice appear to be cognitively normal, lowering total tau levels in neurons appears to be safe and will likely have a high therapeutic index (Morris et al., 2013). Thus, soluble tau is a promising therapeutic target. However, identifying selective, non-toxic tau-lowering compounds has proven to be difficult (Gruninger, 2015).

Cell-based "phenotypic" high-throughput screening (HTS) is a powerful unbiased tool to identify gene targets or small-molecule compounds exerting desired effects. However, HTS requires large numbers of cells and has been largely restricted to immortalized human neuronal lines, such as neuroblastoma SH-SY5Y(Jain et al., 2012) and glioma H4 (Albrecht et al., 2004) cells, or non-neuronal lines, such as HeLa cells (Fatokun et al., 2013). Since these cells differ physiologically from post-mitotic neurons, hits identified in these cells might not work in neurons. This may be particularly true for tau, a neuronal protein that is abundant in axons but is mainly expressed in the cytosol in non-neuronal cells (Uberti et al., 1997). Rodent primary neurons are more physiologically relevant, but challenges in scalability preclude their use for HTS, and certain compounds may differ in activity between human and rodent cells.

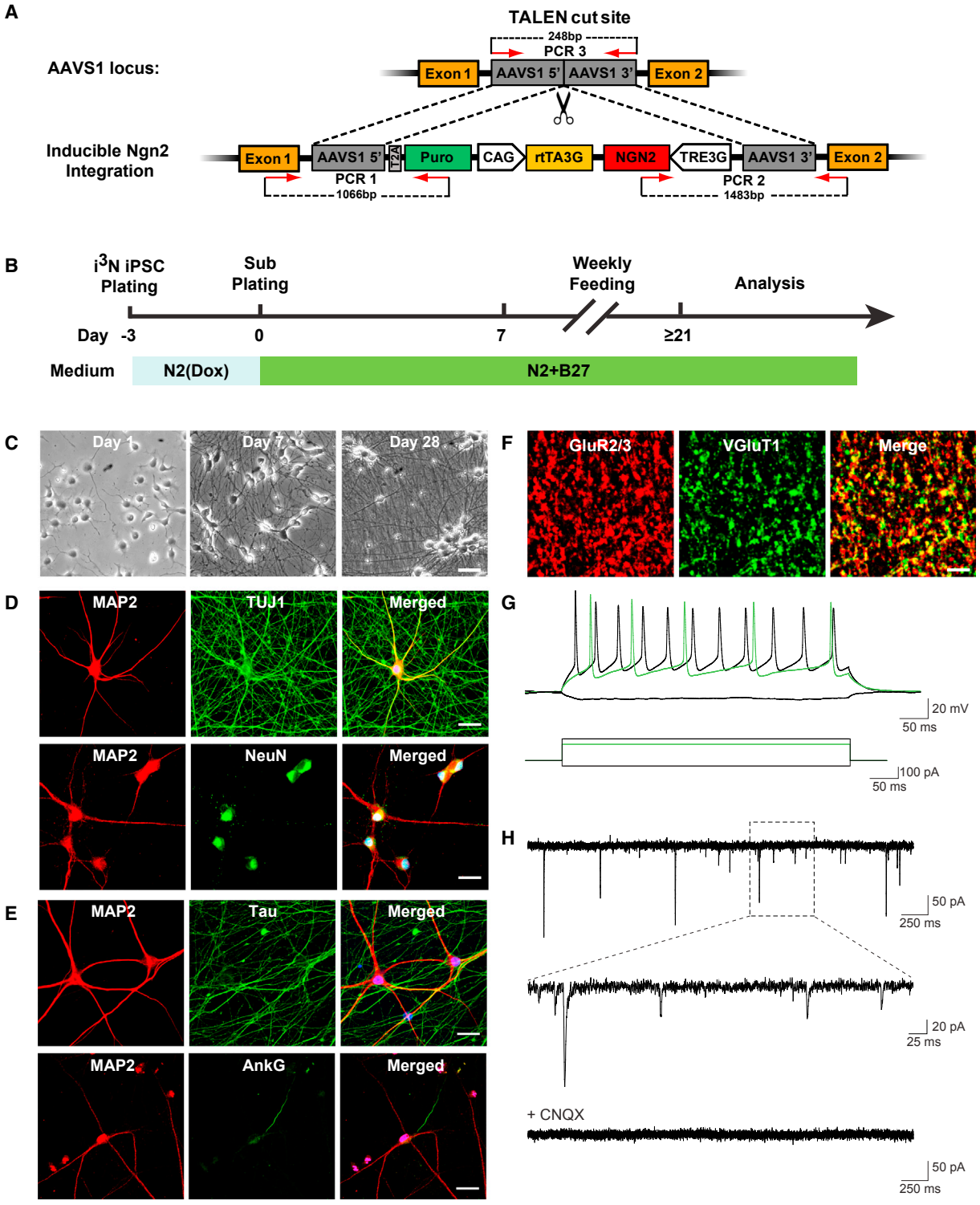

Figure 1. Engineering of i^{3}N iPSCs and Generation of Homogeneous Functional Glutamatergic Neurons by a Simplified Two-Step Procedure

(A) Schematic of the targeting of the AAVS1 locus with pUCM.Puro-CAG.rtTA3G-TRE3G.Ngn2 donor vector by TALEN-mediated integration. The third-generation doxycycline-inducible reverse transcriptional activator (rtTA3G) is driven by the CAG promoter and followed by rbGlob polyA tail. Mouse *Ngn2* is driven by the tet response element (TRE3G) and followed by SV40 polyA tail. It is oriented tail-to-tail with

(legend continued on next page)

Human induced pluripotent stem cells (iPSCs) are a promising alternative because they can be used to generate large numbers of subtype-specific human neurons that are relevant to neurodegenerative disease. However, iPSC-derived neurons currently have limited utility in HTS assays (D'Aiuto et al., 2014), as traditional differentiation methods are difficult to scale up and usually yield a heterogeneous population of neurons and glia-like cells over a protracted timeline (Muratore et al., 2014; Nicholas et al., 2013). More homogeneous neuronal populations can be produced by overexpressing pro-neuronal transcription factors (Chanda et al., 2014; Pang et al., 2011). Neurogenin 2 (NGN2)-induced neurons from various human embryonic stem cell and iPSC lines show robust morphological, transcriptional, and functional homogeneity (Busskamp et al., 2014; Zhang et al., 2013). However, this method has shortcomings for HTS. First, it entails a labor-intensive multi-step differentiation procedure that is difficult to apply to microplates. Second, it is subject to cell-to-cell and well-to-well variability due to different viral infection and puromycin selection rates, uneven cell distribution, which might affect cell survival and image quantification, and experiment-to-experiment variability due to differences in viral titers and qualities of primary mouse glia from different batches. Third, it is costly to scale up.

In this study, we engineered a clonal iPSC line that stably harbors a doxycycline-inducible mouse *Ngn2* transgene at an adeno-associated virus integration site 1 (AAVS1) safe-harbor locus. This integrated, inducible, and isogenic *Ngn2* iPSC line (i^3N) can be differentiated into functional glutamatergic cortical neurons by a simplified two-step differentiation protocol. We developed a robust high-content screening (HCS) assay to identify tau-lowering compounds and discovered compounds that target adrenergic receptor (AR) pathways to lower endogenous human tau.

RESULTS

Engineered iPSCs for Scalable Production of Homogeneous Excitatory Neurons

Lentivirus-mediated NGN2 expression induces rapid differentiation of iPSCs into excitatory neurons (Zhang et al., 2013). To avoid viral transduction-induced toxicity and variability in NGN2 expression, we engineered isogenic iPSC lines with an integrated *Ngn2* expression cassette. A doxycycline-inducible *Ngn2* transgene was integrated into the AAVS1 safe harbor of a well-characterized control human iPSC line (WTC11) (Miyaoka et al., 2014) by TALEN-mediated integration of a donor cassette containing a puromycin-resistance gene (Figure 1A). Six puromycin-resistant clones were picked, and integration of the *Ngn2* transgene into the AAVS1 locus was confirmed with two sets of primers (PCR1 and PCR2) (Figures 1A and S1A). Transgene integration into both alleles was confirmed by the absence of the wild-type allele, determined by a third set of primers (PCR3) (clones 1 and 4). These iPSC clones have isogenic, integrated, and inducible NGN2 expression (i^3N); neurons derived from them are called i^3Neurons. Further characterization of clone 1 in the absence of doxycycline showed homogeneous expression of the pluripotency markers OCT4, SOX2, and TRA-1-81, indicating no leakage of NGN2 expression (Figure S1B). The cells also had a normal karyotype (Figure S1C).

i^3N iPSCs could be differentiated into functional excitatory neurons by the published multi-step differentiation protocol. To overcome the poor scalability and reproducibility of this procedure when adapted to the HTS platform, we established a simplified two-step protocol (Figure 1B). After doxycycline induction and subplating, pre-differentiated i^3Neurons became post-mitotic, and

rtTA3G. Orange boxes are exons of the PPP1R12C gene; gray boxes are regions of homology. PCR1 and PCR2 primers are used for 5′ and 3′ junction PCR screening and generate 1.1-kb and 1.5-kb PCR products, respectively. PCR3 primers (product size, 248 base pairs) are used to detect the nonintegrated allele at the AAVS1 locus.

(B) Flow diagram of the two-step procedure for generating i^3Neurons.

(C) Representative phase-contrast images during the differentiation of i^3Neurons. The timeline is the same as shown in (B). Scale bar, 50 μm.

(D) Representative images showing immunocytochemical staining for the pan-neuronal marker MAP2, βIII tubulin (TUJ1 antibody), and NeuN in i^3Neurons after 4 weeks of differentiation. Nuclei were labeled by Hoechst. Scale bar, 25 μm.

(E) Representative images of immunocytochemical staining of mature 8-week-old i^3Neurons show tau enrichment (detected with HT7) in an axon identified by the axon initiation segment marker ankyrin G (AnkG). Nuclei were labeled by Hoechst. Scale bar, 25 μm.

(F) Representative confocal images of i^3Neurons showing immunolabeling of postsynaptic GluR2/3 containing AMPA-type glutamate receptors (red) and the presynaptic vesicular glutamate transporter VGlut1 (green). The colocalization of GluR2/3 and VGlut1 puncta marks glutamatergic synapses formed between i^3Neurons. Scale bar, 5 μm.

(G) Representative traces of action potentials evoked by 500-ms current step injections at just above the firing threshold (green trace) and at a higher firing frequency (black trace).

(H) Spontaneous excitatory postsynaptic currents recorded from an i^3N neuron (top) were blocked by CNQX, an AMPA receptor antagonist (bottom).

See also Figures S1 and S2.

exhibited neuron-like morphology in less than 7 days and mature neuronal morphology within 3–4 weeks in the absence of glia (Figure 1C). Differentiated neuron markers βIII tubulin (TUJ1), microtubule-associated protein 2 (MAP2), and neuronal nuclei antigen (NeuN) were detected in i^{3}Neurons after 4 weeks of maturation (Figure 1D). The absence of Olig2-positive oligodendrocytes or glial fibrillary acidic protein (GFAP)-positive astrocytes confirmed the purity of the neuronal population (Figure S2A).

In 8-week-old i^{3}Neurons, tau was abundant in axons identified by the presence of a single axonal initial segment (AIS), as detected with ankyrin G staining (Kordeli et al., 1995) (Figure 1E). More than 90% of i^{3}Neurons contained AIS, supporting the notion that they exhibit mature polarity by 8 weeks (Figure S2B). Tau expression had little overlap with MAP2, a dendritic marker (Figure 1E). Both three-repeat (3R) and four-repeat (4R) tau were detected (Figure S2C). Tau in i^{3}Neurons were also highly phosphorylated, compared with healthy human brain (Figure S2D). Importantly, all i^{3}Neurons expressed vesicular glutamate transporter 1 (VGlut1), a marker of glutamatergic neurons, and were GABA negative, indicating a homogeneous population of excitatory glutamatergic neurons (Figure S2E). The punctate distribution of synapsin-1 staining along the processes revealed abundant synapse formation (Figure S2F). When co-cultured with glia, i^{3}Neurons had mature synapses that contained juxtaposed pre- and postsynaptic markers of glutamatergic synapses (Figure 1F). Whole-cell patch-clamp recordings showed action potential firing in response to current injections (Figure 1G). Spontaneous postsynaptic currents detected in i^{3}Neurons were blocked by CNQX, an AMPA receptor antagonist, confirming functional glutamatergic synaptic transmission (Figure 1H).

i^{3}Neurons Cultured in Microplates Show Homogeneous Gene Expression with Low Variability

Two key determinants of reliable HTS are scalability and minimal well-to-well variability. We were able to produce large quantities of i^{3}Neurons via i^{3}N iPSC proliferation and a pre-differentiation step. Subsequent subplating enables i^{3}Neurons culture in 96- and 384-well microplates with even cell distribution (Figure 1B). To determine whether i^{3}Neurons homogeneously differentiate in microplates, we quantified the expression of multiple neuronal and glial genes of 4-week-old cells from 12 randomly selected wells of a 96-well plate by RT-qPCR (Figure 2). Consistently high levels of pan-neuronal genes, AMPA receptor genes, glutamate transporter genes, synaptic genes, and *CUX1*, a marker of cortical layer 2/3 neurons, were observed in all 12 wells, suggesting a uniform differentiation of glutamatergic cortical neurons. In addition, all the i^{3}Neurons showed low expression of two markers of neural progenitor cells, *PAX6* and *NESTIN*, indicating that they were fully differentiated. *Ngn2* was undetectable, as expected in the absence of doxycycline. No markers of glial cells or of GABAergic neurons (e.g., *GAD65/67*) were detected, but the GABA receptors *GABRA2* and *GABRB1* were expressed at low levels. Thus, i^{3}Neurons can be cultured in microplates with low well-to-well variability and are suitable for HTS.

Optimization of an HCS Assay to Screen for Tau-Lowering Compounds

Lowering tau levels has emerged as a key therapeutic opportunity in AD. To our knowledge, no HCS targeting endogenous tau has been performed in post-mitotic human neurons. Because i^{3}Neurons are scalable and highly homogeneous, they are an ideal system to screen for tau-targeted therapeutics. Taking advantage of the highly specific anti-human tau antibody HT7, we set out to develop a 384-well format HCS assay to detect endogenous tau levels in i^{3}Neurons (Figure 3A). Total tau levels were determined by immunoreactivity of HT7 normalized to βIII tubulin intensity in a corresponding well (HT7/TUJ1) (Figure 3B). The background signal, measured in wells omitting HT7, was more than 10-fold lower than those with HT7 (Figures 3B and S3A). The optimal seeding density was 2,000 cells/well (Figure S3A). Neuronal health was judged from neurite total length (Figure S3B) and valid nucleus count (Figure S3C), two highly correlated health parameters (Figure S3D) that are widely used (Harrill et al., 2013; K Hancock et al., 2015). Treatment with a tau-specific siRNA reduced the total tau levels in a dose-dependent manner (Figures 3C and 3D), whereas increased total tau levels were detected when i^{3}Neurons were infected by AAV human tau (Figures S3E and S3F), confirming assay specificity and sensitivity. Salicylate, YM-01, and methylene blue reduce total tau levels (Abisambra et al., 2013; Hosokawa et al., 2012; Min et al., 2015). All three compounds reduced the HT7/TUJ1 signal in a time-dependent manner accompanied by a mild yet significant reduction of neurite total length (Figure 3E). The Z′ factor, a measure of the assay response window (Zhang et al., 1999) and determined by values of control and hTau siRNA, was 0.41, supporting the robustness of the HCS assay.

Identification of Tau-Lowering Compounds via HCS

Next, we used the HCS assay to screen LOPAC (Library of Pharmacologically Active Compounds) for tau-lowering compounds. This library contains 1,280 bioactive small molecules, including inhibitors, receptor ligands, marketed drugs, and pharmaceutically relevant structures, that affect most signaling pathways and cover major drug target classes. Since overwhelming majority compounds did not change tau levels (Figure 4A), we used sample compounds

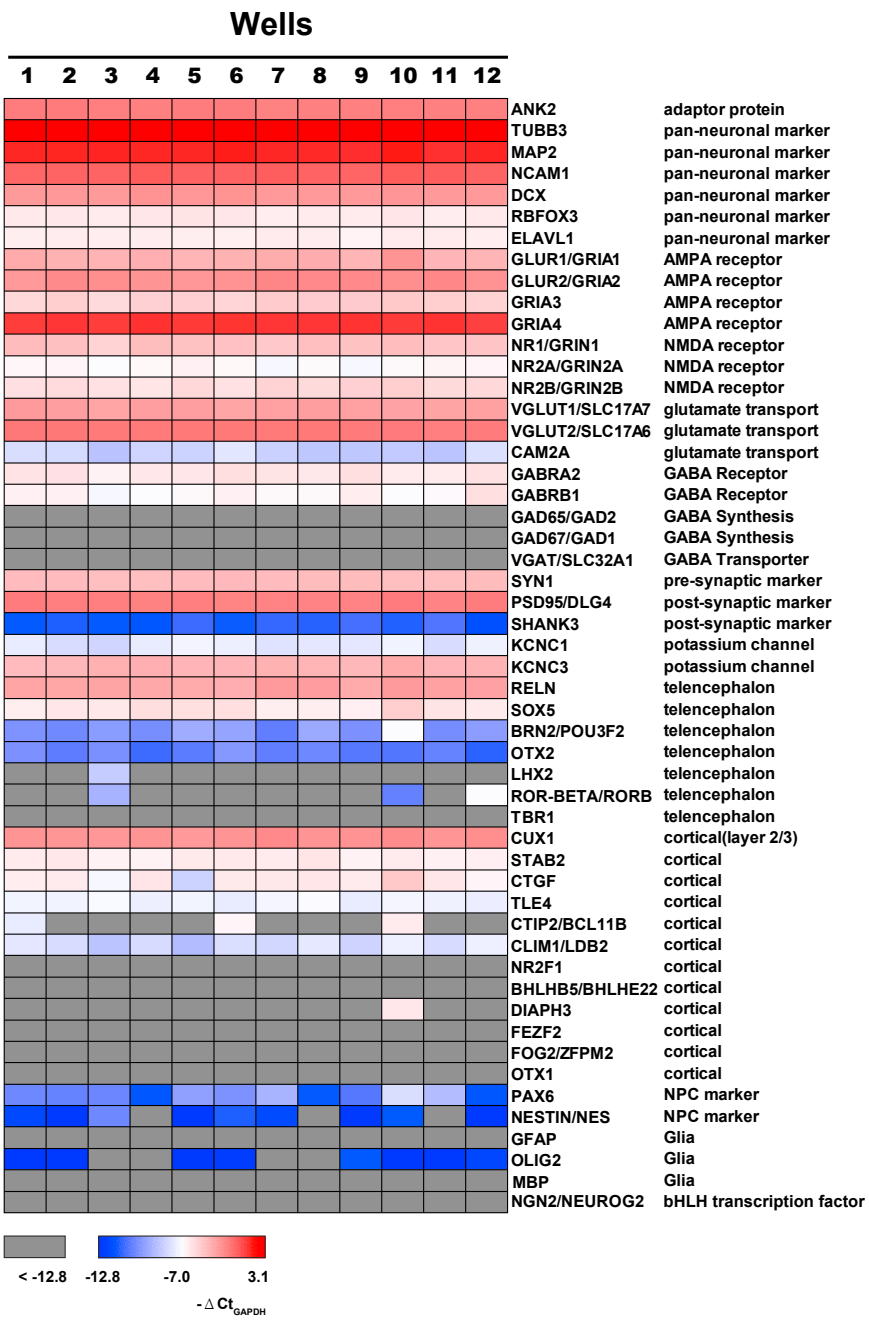

Figure 2. i^{3}Neurons Show Homogeneous Expression of Glutamatergic Cortical Neuronal Genes

Heatmap of RT-qPCR analysis of expression levels of genes listed on the right. Expression levels are normalized to housekeeping gene *GAPDH* (expressed as $-\Delta$Ct) and color coded as shown. mRNA was harvested from 12 random wells of 4-week-old i^{3}Neurons cultured in a 96-well plate. See also Table S1.

as their own control and calculated Z scores based on LOPAC compounds on each plate (Brideau et al., 2003). Compounds that changed tau (as judged from the HT7/TUJ1 ratio) were defined as hits if their Z scores were greater than 3 or less than −3, a stringent cut-off correlates to a p value of 0.00135 (Zhang et al., 2006). All hits were then ranked by neuronal health parameters, including neurite total length (Figure 4B) and valid nucleus count (Figure 4C).

The top two tau-lowering hits that show least cytotoxicity, measured by neurite total length and valid nucleus count, are two functionally related AR agonists, moxonidine and metaproterenol (Figures 4B and 4C). To validate these hits, we adapted a sensitive human tau ELISA that uses HT7 as the capture antibody and Tau5 as the detection antibody (Meredith et al., 2013). The dynamic range of the assay was >3,000, and the detection limit was ~10.7 pg/mL (Figure 5A). This assay readily detected siRNA-induced reduction of endogenous human tau by >50% (Figure 5B). We then confirmed that moxonidine, clonidine (a moxonidine-related adrenergic agonist), and

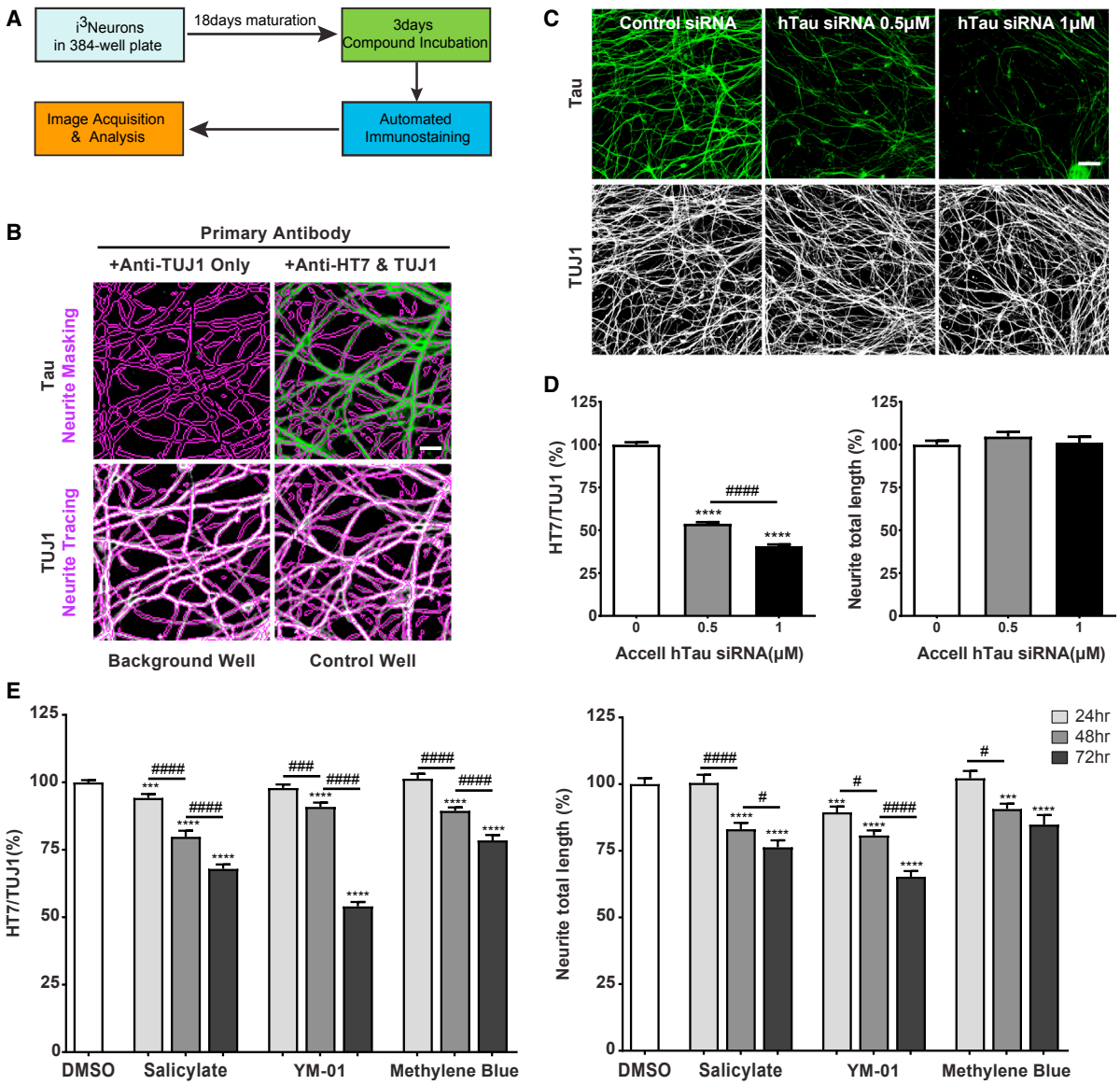

Figure 3. Development and Validation of an HCS Assay to Detect Tau Levels in i^{3}Neurons

(A) Schematic of the HCS assay optimized to measure cellular tau levels in neurons treated with small-molecule compounds.

(B) Representative fluorescence high-content images showing tau (green) and βIII tubulin (white) channels from a background well (left, anti-TUJ1 only) and a control well (right, anti-HT7 and TUJ1). Neurite regions (purple) were traced according to the TUJ1 channel and were applied to the tau channel with the neuronal profiling module of Cellomics software. Scale bar, 10 μm.

(C) Representative fluorescence high-content images showing tau (green) and βIII tubulin (white) channels from i^{3}Neurons after 7 days of treatment with control siRNA or human tau siRNA (0.5 or 1 μM). Scale bar, 50 μm.

(D) Automated quantification of human tau levels (left) and neurite total length (right) from i^{3}Neurons treated with human tau siRNA. Data are from three independent experiments, total N = 42 per treatment; values are means ± SEM relative to control siRNA. ****p < 0.0001 compared with control siRNA, STATA mixed model. ####p < 0.0001, STATA mixed model.

(E) Automated quantification of human tau levels (left) and neurite total length (right) from i^{3}Neurons treated with 5 mM salicylate, 1 μM YM-01, or 1.5 μM methylene blue for 24–72 hr. Data are from three independent experiments, total N = 42 per treatment; values are means ± SEM relative to DMSO. ***p < 0.001, ****p < 0.0001, compared with DMSO, STATA mixed model; #p < 0.05, ###p < 0.001, ####p < 0.0001, comparison between three time points within each compound treatment, STATA mixed model.

See also Figure S3.

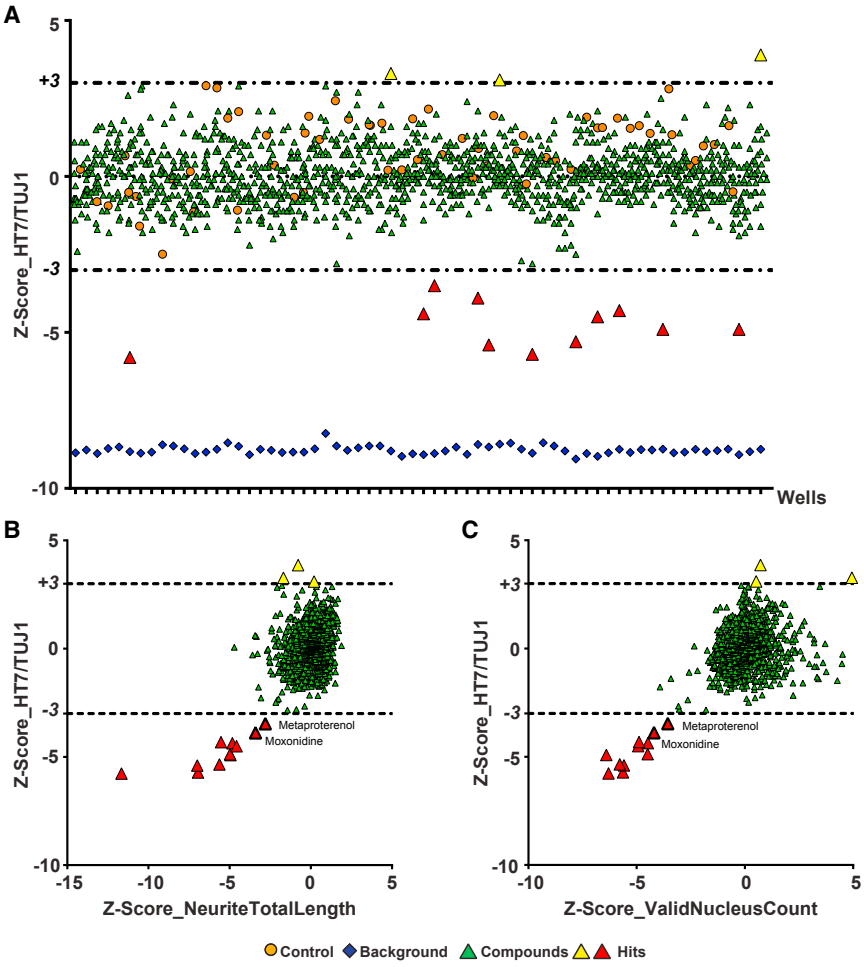

Figure 4. Primary Screening and Hit Selection from LOPAC

(A) Overview of automated quantification of human tau levels from i^{3}Neurons incubated with compounds from LOPAC at 10 μM for 3 days (green triangles). The library was distributed to three and one-half 384-well plates; each plate contains 16 control wells (DMSO, orange circles) and 16 background wells (blue diamonds). Results are shown as the *Z* score, calculated based on LOPAC compounds on each plate. Compounds above (yellow triangles) and below (red triangles) the cut-offs of +3 or −3 (dotted lines) are considered hits.

(B and C) Hits are ranked by neurite total length (B) and valid nucleus count (C). Results are shown as *Z* score, calculated based on LOPAC compounds on each plate. Moxonidine and metaproterenol are the top two tau-lowering hits from both rankings.

metaproterenol reduced tau levels in a dose-dependent manner. None of the three compounds induced a significant loss of βIII tubulin, as measured with a βIII tubulin ELISA, indicating a lack of toxicity (Figures 5C–5E).

Additional pharmacologic modulators of α- and β-AR activity were used to further confirm the involvement of α- and β-adrenergic signaling in modulating endogenous human tau levels. i^{3}Neurons were treated with nonselective α- or β-AR agonists (dexmedetomidine or isoproterenol) and their respective antagonists. Activation of α- or β-ARs significantly reduced endogenous human tau levels, and inhibition by nonselective antagonists caused tau accumulation (Figures 5F and 5G). Moreover, the tau-lowering effects of moxonidine and metaproterenol were abolished by pre-incubation with the corresponding antagonists (atipomezole and propranol, respectively) (Figures 5F and 5G). The ability of α- or β-AR agonists to reduce endogenous tau levels was further confirmed in an independent line of i^{3}Neurons (Figures S4A and S4B). Our results showed that activation of α- and β-adrenergic signaling pathways could represent tau-lowering therapeutic strategies in human neurons.

DISCUSSION

In this study, we integrated a doxycycline-inducible mouse *Ngn2* cassette into the AAVS1 locus and established iPSC lines that can be converted efficiently to a uniform population of glutamatergic neurons by a simplified two-step protocol. We then developed a robust, scalable, and simple HCS assay and used it to identify compounds that lower tau in post-mitotic human neurons. This proof-of-principle screen identified AR agonists as a class of compounds that decrease endogenous human tau levels.

i^{3}Neurons have several features that make them suitable for HTS, particularly imaging-based HCS. First, the population of differentiated neurons is homogeneous, which may reflect the uniform genetic background of the clonal i^{3}N iPSCs. As all of the iPSC-derived cells are neurons,

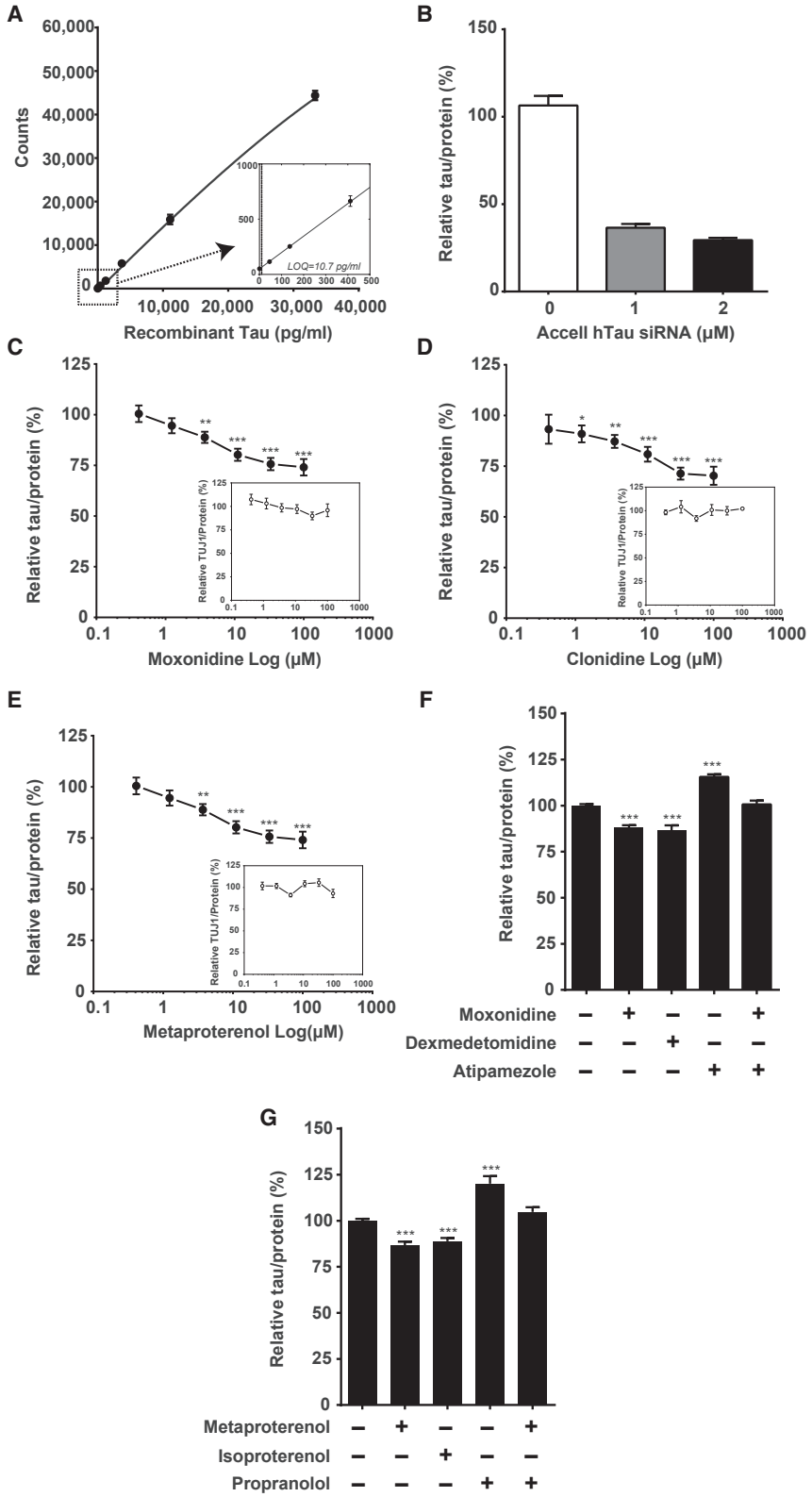

Figure 5. Activation of α- and β-AR Reduces Total Tau Levels in i^{3}Neurons

(A) Representative calibration curve of HT7-Tau5 ultra-sensitive human tau ELISA. Inset shows the assay's limit of quantification (LOQ).

(B) 7-day incubation of human tau siRNA significantly lowered total tau levels in i^{3}Neurons. Human tau levels were quantified by HT7-Tau5 ELISA and normalized to protein level. Values are means ± SEM relative to control siRNA. Data are from one experiment, N = 6 wells per treatment.

(C–E) Concentration-response curve of moxinidine (C), clonidine (D), and metaproterenol (E) determined by HT7-Tau5 ELISA. Insets show the βIII tubulin level for each concentration as determined by βIII tubulin ELISA. Both tau and βIII tubulin levels are normalized to protein levels. Values are means ± SEM relative to DMSO control. Data are from four independent experiments performed in triplicate (C, N = 12 per concentration) and three independent experiments performed in triplicate (D and E, N = 9 per concentration). *$p < 0.05$, **$p < 0.01$, ***$p < 0.001$; STATA mixed model.

(F and G) 3-day incubation with moxonidine (30 μM) and the α-AR agonist dexmedetomidine (100 μM) (F) or metaproterenol (30 μM) and the β-AR agonist isoproterenol (30 μM) (G) significantly reduced total tau levels in i^{3}Neurons. The α-AR antagonist atipamezole (100 μM) (F) and the β-AR antagonist propranolol (50 μM) (G) increased total tau levels and abolished the tau-lowering effect of moxonidine (F) or metaproterenol (G), respectively. Human tau levels were quantified by HT7-Tau5 ELISA and normalized to protein level. Values are means ± SEM relative to DMSO control. Data are from three independent experiments performed in triplicate (F, N = 9 per treatment) and four independent experiments performed in triplicate (G, N = 12 per treatment) ***$p < 0.001$, STATA mixed model.

See also Figure S4.

sensitivity and specificity of HTS screens is increased. Other safe-harbor loci besides the AAVS1 locus (e.g., citrate lyase beta-like) can be used in human iPSCs (Cerbini et al., 2015). By targeting multiple safe-harbor sites with P2A or IRES elements, it may be possible to integrate multiple inducible transcription factors to differentiate iPSCs into other neuronal subtypes, such as dopaminergic neurons (Amamoto and Arlotta, 2014) or motor neurons (Hester et al., 2011), for use in HTS. Second, our simplified glia-free differentiation protocol overcomes hurdles, such as scalability, variability, complexity, and cost, that previously hindered the use of iPSC-derived neurons in drug discovery pipelines. For example, instead of generating and freezing large quantities of neuronal precursor cells, our approach involves a single cost-effective 3-day pre-differentiation procedure. The pre-differentiated neurons are post-mitotic and can be subplated onto poly-D-lysine/laminin-coated microplates with high consistency. Differentiation of i^3Neurons does not require viral infection, puromycin selection, or frequent medium change, thereby reducing the possibility of introducing variability and contamination during HTS. Thus, standardized HTS procedures can be established regardless of location, time, or users, facilitating future use of i^3Neurons for ultra-HTS of large libraries of chemical compounds.

Tau-targeted approaches have been proposed as an alternative therapeutic strategy for AD and other tauopathies (Dehdashti et al., 2013; DeVos et al., 2013; Panza et al., 2016). Previous tau-targeted small-molecule strategies—including kinase inhibitors against hyperphosphorylated tau, tau aggregation inhibitors, microtubule stabilizers, and compounds that enhance clearance of tau aggregates—have had limited success (Brunden et al., 2009; Gruninger, 2015; Medda et al., 2016; Min et al., 2015; Panza et al., 2016). Lowering total tau levels may have beneficial effects. For example, the MAPT H1c haplotype increases tau expression and is associated with increased risk of progressive supranuclear palsy, corticobasal degeneration, and AD (Baker et al., 1999; Di Maria et al., 2000; Myers et al., 2005, 2007). Tau lowering in transgenic mouse models rescued functional deficits and tau-mediated neurodegeneration (Andrews-Zwilling et al., 2010; Ittner et al., 2010; Lasagna-Reeves et al., 2016; Min et al., 2015; Roberson et al., 2007, 2011; Vossel et al., 2010) and appears to be safe (Morris et al., 2013). However, discovering compounds that reduce total tau levels has been challenging. Tau is natively unstructured and has proved a difficult target for rational drug design. Several tau-lowering candidates that reduce tau gene transcription were identified by small-scale screening with in-cell western analysis (Dickey et al., 2006). AlphaLISA and homogeneous time-resolved fluorescence assays were used in SH-SY5Y cells to screen for tau-lowering compounds (Dehdashti et al., 2013). However, these studies were done and validated only in tumor cell lines that lack well-defined axons highly enriched in tau. Previous tau-lowering compounds also caused significant cytotoxicity (Dehdashti et al., 2013). In addition, the regulation of tau homeostasis may differ in rodent and human neurons. Indeed, methylene blue, which reduces the levels of human tau overexpressed in mouse neurons *in vivo* and *in vitro* (Congdon et al., 2012; Hosokawa et al., 2012), had minor effect in human neurons in our assay.

Using i^3Neurons in a robust HCS assay, we identified AR agonists as a class of tau-lowering compounds. Both α- and β-AR signaling appeared to regulate tau levels in similar fashion, as AR activation led to tau reduction and AR inhibition led to tau accumulation. Besides moxonidine hydrochloride (α-adrenergic agonist) and metaproterenol hemisulfate (β-adrenergic agonist), three other α- or β-adrenergic agonists (clonidine, dexmedetomidine, and isoproterenol) also reduced tau levels in human neurons. The tau-lowering effects of moxonidine and metaproterenol were abolished by their corresponding antagonists atipomezole and propranol, which elevated tau levels by themselves. In agreement with our findings, the selective β2-AR antagonist ICI 118,551 increased tau phosphorylation and accumulation in an AD mouse model (Branca et al., 2014). Paradoxically, genetic suppression of β2-ARs reduced tau pathology (Wisely et al., 2014). One likely explanation could be that complete removal of β2 AR prevented harmful effects of dysregulated β2-ARs, such as binding to Aβ.

Deficiency in α- or β-AR signaling has been implicated in AD. Levels of high-affinity α2-ARs are markedly reduced in AD patients (Pascual et al., 1992). Polymorphisms of β-ARs are linked to increased risk of late-onset AD (Yu et al., 2008). The natural ligand of ARs is norepinephrine, whose major source in the CNS is noradrenergic neurons in the locus coeruleus (LC); these neurons project widely to the forebrain, which includes two regions especially affected by tauopathies, the hippocampus and neocortex (Mather and Harley, 2016). Patients with AD have significant degeneration of neurons in the LC and much lower levels of norepinephrine. Interestingly, abnormal tau lesions emerged predominantly in LC regions even in individuals in their 20s, 30s, and 40s (Braak and Del Trecidi, 2015; Braak et al., 2011), suggesting that low levels of norepinephrine in the LC may lead to tau accumulation in young susceptible people and can eventually propagate to other brain regions.

How adrenergic signaling affects tau homeostasis is not known. Interestingly, some AR-modulating compounds may have a beneficial effect that is independent of their AR agonist activities. For example, norepinephrine and isoproterenol, whose chemical backbones contain 1,2-dihydroxybenzene, reduce insoluble tau levels by directly binding cysteine residues in tau to prevent tau oligomerization, independent of their AR agonist activities (Soeda

et al., 2015). Modulating adrenergic signaling could affect other aspects of AD pathology as well. Chronic activation of β-ARs increases Aβ production (Ni et al., 2006) and protects against the detrimental effects of Aβ on hippocampal function (Li et al., 2013). AR activation also reduces lipopolysaccharide-induced expression of tumor necrosis factor alpha in microglia (Schlachetzki et al., 2010; Szabo et al., 1997) and interferon-γ-induced expression of class II antigens in astrocytes (Frohman et al., 1988). More studies are needed to dissect the molecular mechanisms underlying the role of adrenergic signaling in AD and to further validate AR agonists as a potential therapeutic strategy for AD and related tauopathies.

EXPERIMENTAL PROCEDURES

Chemicals and Reagents

All medium, reagents, and supplements for iPSC culture and differentiation were from Invitrogen unless otherwise specified. Doxycycline, DMSO, cytosine β-D-arabinofuranoside (Ara-C), salicylate, LOPAC library, AR agonists and antagonists, and electrophysiology related chemicals were from Sigma.

Generating and Selecting i^{3}N iPSC Clones

Ngn2 transgene was subcloned to a pUCM donor vector containing an AAVS1 homology arm. The Tet-ON 3G-controlled *Ngn2* transgene was integrated to the AAVS1 locus of human iPSC lines through a TALEN nuclease pair. Genomic DNA from puromycin-selected and expanded clones were purified and genotyped by three PCR reactions. We generated i^{3}N iPSC lines from two independent wild-type genetic background human iPSC lines: WTC11 (Miyaoka et al., 2014) and F12486.13 (female, white, age at biopsy 48 years, reprogrammed by Sendai virus, generated by Dr. Celeste Karch, Washington University in St. Louis). The iPSC protocol was approved by the Committee on Human Research at the University of California, San Francisco (15-15798). A detailed protocol is described in Supplemental Experimental Procedures.

i^{3}Neuron Differentiation

i^{3}Neurons were differentiated with a simplified two-step protocol (pre-differentiation and maturation). For pre-differentiation, i^{3}N iPSCs were incubated with doxycycline (2 μg/mL) for 3 days at a density of 2.0–2.5 × 10^6 cells/well in six-well plates coated with Matrigel in knockout Dulbecco's modified Eagle's medium (KO-DMEM)/F12 medium containing N2 supplement, non-essential amino acids (NEAA), mouse laminin (0.2 μg/mL), brain-derived neurotrophic factor (BDNF, 10 ng/mL), neurotrophin-3 (NT3,10 ng/mL; Peprotech), and Y-27632. The medium was changed daily, and Y-27632 was removed from day 2. For maturation, pre-differentiated i^{3}N precursor cells were dissociated, counted, and subplated at the desired density on plates coated with poly-D-lysine (PDL)/laminin in maturation medium containing 50% DMEM/F12, 50% Neurobasal-A medium, 0.5× B27 supplement, 0.5× N2 supplement, GlutaMax, NEAA, mouse laminin (1 μg/mL), BDNF (10 ng/mL), and NT3 (10 ng/mL). Half of the medium was replaced on day 7 and again on day 14, and the medium volume was doubled on day 21. Thereafter, one-third of the medium was replaced weekly until the cells were used. For electrophysiological recording, i^{3}N precursor cells were subplated on Matrigel-coated coverslips, and mouse glia were added on day 1 in maturation medium containing 5% heat-inactivated fetal bovine serum and 2 μM Ara-C.

Immunocytochemistry

i^{3}N iPSCs or i^{3}Neurons in coverslips were fixed with conditioned medium containing 4% paraformaldehyde, permeabilized with 0.1% Triton X-100, and incubated for 1 hr in blocking solution containing PBS, 0.01% Triton X-100, and 5% normal goat serum. The cells were then incubated in blocking solution containing primary antibody overnight at 4°C, followed by incubation with secondary antibody for 1 hr. Images were acquired with an LSM880 confocal system (Zeiss) with Airyscan and a 20× or 63× oil-immersion objective lens. Antibodies used for immunocytochemistry were those against SOX2 (sc-17320S; Santa Cruz Biotechnology), OCT4 (sc-5279; Santa Cruz Biotechnology), TRA-1-81 (sc-21706; Santa Cruz Biotechnology), MAP2 (AB5622 or MAB3418; Millipore), VGlut1 (MAB5502; Millipore), βIII tubulin (TUJ1; Aves Labs), neuronal nuclear antigen (MAB377; Millipore), GABA (A2052; Sigma), HT7 (MN1000; Thermo Fisher), ankyrin G (N106/36; NeuroMa), synapsin-1 (D12G5; Cell Signaling), Olig2 (AB9610; Millipore), GFAP (MAB3402; Millipore), and GluR2/3 (AB1506; Millipore).

Reverse Transcription and Real-Time qPCR

i^{3}Neurons were cultured in 96-well PDL plates (655946, Greiner) at a density of 10,000 cells/well for 4 weeks. cDNA from 12 random wells was obtained with Cells-to-CT Kits (Ambion) as recommended by the manufacturer. qPCR reactions were done in duplicate with SYBR Green Real-Time PCR master mixes (Applied Biosystems) and the Applied Biosystems 7900HT fast real-time PCR system. All the primers (Table S1) have been validated with human brain RNA (Zhang et al., 2013). RNAs without reverse transcription were used as negative control, and the dissociation curve from each gene was reviewed to ensure the desired amplification. Expression levels were normalized to *GAPDH*.

HCS Assay to Determine Total Tau Levels

After pre-differentiation, i^{3}N precursor cells were placed in 384-well plates at a density of 2,000 cells/well. Fresh maturation medium was added weekly. On day 18, human tau siRNA, known tau-lowering compounds (salicylate, YM-01, and methylene blue) and 1,280 compounds from LOPAC were added and incubated at the desired final concentration for the desired amount of time. Human tau, recognized by HT7 antibody, total neurites, recognized by βIII tubulin antibody (TUJ1; Aves Labs) and nuclei, recognized by Hoechst were detected by a semi-automated immunostaining procedure. A fully automated ArrayScan high-content system (Thermo) was used to acquire images and quantify total tau levels. See Supplemental Experimental Procedures for detailed methods.

Human Tau and βIII Tubulin ELISA

Sensitive human tau and βIII tubulin ELISAs were adapted and modified according to previous reports (Barten et al., 2011;

Meredith et al., 2013). Briefly, mouse monoclonal antibody HT7 or rabbit monoclonal βIII tubulin antibody (ab68193; Abcam) was used for capture. The respective analytes were detected with alkaline phosphatase-conjugated mouse monoclonal antibodies Tau5 or TUJ1 (806401, 801201; BioLegend). Recombinant full-length human tau (rPeptide) and recombinant βIII tubulin (Cytoskeleton) were used to generated standard curves for each assay. The CDP-Star substrate (T2214, Invitrogen) was used as a chemiluminescent alkaline phosphatase substrate. See Supplemental Experimental Procedures for detailed methods.

Statistics

The sample size for each experiment was determined on the basis of previous experience. Differences between means were assessed by unpaired Student's t test (GraphPad Prism, v. 6.0) or multilevel mixed-effects linear regression model (STATA12; StataCorp), as indicated. Values are reported as means ± SEM. The Shapiro-Wilk test of normality and F test to compare variances were applied to datasets when applicable.

SUPPLEMENTAL INFORMATION

Supplemental Information includes Supplemental Experimental Procedures, four figures, and one table and can be found with this article online at http://dx.doi.org/10.1016/j.stemcr.2017.08.019.

AUTHOR CONTRIBUTIONS

L.G., M.E.W., and C.W. conceived the project and designed the experiments. C.W., M.E.W., R.C., K.L., T.E.T., X.C., P.D.S., and C.L. performed the experiments and collected and analyzed the data. M.X., A.M.-F., and D.S. contributed to data analyses and interpretation. C.M.K. generated the original F12486.13 iPSC line. C.W., M.E.W., and L.G. wrote the manuscript.

ACKNOWLEDGMENTS

We thank B. Conklin and M.A. Mandegar for the WTC11 line and the pUCM donor vector, T.C. Südhof and Y. Zhang for the mouse *Ngn2* plasmid and differentiation protocol, S. Ordway and G. Howard for editorial assistance, and E. Nyguen for administrative assistance. This work was supported in part by NIH R01AG036884 and R01AG051390 and the Rainwater Foundation to L.G., NIH K08EY023610 to M.E.W., and NIH K01AG046374 to C.M.K.

Received: March 8, 2017
Revised: August 25, 2017
Accepted: August 28, 2017
Published: September 28, 2017

REFERENCES

Abisambra, J., Jinwal, U.K., Miyata, Y., Rogers, J., Blair, L., Li, X., Seguin, S.P., Wang, L., Jin, Y., Bacon, J., et al. (2013). Allosteric heat shock protein 70 inhibitors rapidly rescue synaptic plasticity deficits by reducing aberrant tau. Biol. Psychiatry *74*, 367–374.

Albrecht, H., Zbinden, P., Rizzi, A., Villetti, G., Riccardi, B., Puccini, P., Catinella, S., and Imbimbo, B.P. (2004). High throughput screening of beta-amyloid secretion inhibitors using homogenous time-resolved fluorescence. Comb. Chem. High Throughput Screen. *7*, 745–756.

Amamoto, R., and Arlotta, P. (2014). Development-inspired reprogramming of the mammalian central nervous system. Science *343*, 1239882.

Andorfer, C., Acker, C.M., Kress, Y., Hof, P.R., Duff, K., and Davies, P. (2005). Cell-cycle reentry and cell death in transgenic mice expressing nonmutant human tau isoforms. J. Neurosci. *25*, 5446–5454.

Andrews-Zwilling, Y., Bien-Ly, N., Xu, Q., Li, G., Bernardo, A., Yoon, S.Y., Zwilling, D., Yan, T.X., Chen, L., and Huang, Y. (2010). Apolipoprotein E4 causes age- and Tau-dependent impairment of GABAergic interneurons, leading to learning and memory deficits in mice. J. Neurosci. *30*, 13707–13717.

Baker, M., Litvan, I., Houlden, H., Adamson, J., Dickson, D., Perez-Tur, J., Hardy, J., Lynch, T., Bigio, E., and Hutton, M. (1999). Association of an extended haplotype in the tau gene with progressive supranuclear palsy. Hum. Mol. Genet. *8*, 711–715.

Barten, D.M., Cadelina, G.W., Hoque, N., DeCarr, L.B., Guss, V.L., Yang, L., Sankaranarayanan, S., Wes, P.D., Flynn, M.E., Meredith, J.E., et al. (2011). Tau transgenic mice as models for cerebrospinal fluid tau biomarkers. J. Alzheimers Dis. *24* (*Suppl 2*), 127–141.

Braak, H., and Del Trecidi, K. (2015). Neuroanatomy and pathology of sporadic Alzheimer's disease. Adv. Anat. Embryol. Cell Biol. *215*, 1–162.

Braak, H., Thal, D.R., Ghebremedhin, E., and Del Tredici, K. (2011). Stages of the pathologic process in Alzheimer disease: age categories from 1 to 100 years. J. Neuropathol. Exp. Neurol. *70*, 960–969.

Branca, C., Wisely, E.V., Hartman, L.K., Caccamo, A., and Oddo, S. (2014). Administration of a selective beta2 adrenergic receptor antagonist exacerbates neuropathology and cognitive deficits in a mouse model of Alzheimer's disease. Neurobiol. Aging *35*, 2726–2735.

Brideau, C., Gunter, B., Pikounis, B., and Liaw, A. (2003). Improved statistical methods for hit selection in high-throughput screening. J. Biomol. Screen. *8*, 634–647.

Brunden, K.R., Trojanowski, J.Q., and Lee, V.M. (2008). Evidence that non-fibrillar tau causes pathology linked to neurodegeneration and behavioral impairments. J. Alzheimers Dis. *14*, 393–399.

Brunden, K.R., Trojanowski, J.Q., and Lee, V.M. (2009). Advances in tau-focused drug discovery for Alzheimer's disease and related tauopathies. Nat. Rev. Drug Discov. *8*, 783–793.

Busskamp, V., Lewis, N.E., Guye, P., Ng, A.H., Shipman, S.L., Byrne, S.M., Sanjana, N.E., Murn, J., Li, Y., Li, S., et al. (2014). Rapid neurogenesis through transcriptional activation in human stem cells. Mol. Syst. Biol. *10*, 760.

Cerbini, T., Funahashi, R., Luo, Y., Liu, C., Park, K., Rao, M., Malik, N., and Zou, J. (2015). Transcription activator-like effector nuclease (TALEN)-mediated CLYBL targeting enables enhanced transgene expression and one-step generation of dual reporter human

induced pluripotent stem cell (iPSC) and neural stem cell (NSC) lines. PLoS One *10*, e0116032.

Chanda, S., Ang, C.E., Davila, J., Pak, C., Mall, M., Lee, Q.Y., Ahlenius, H., Jung, S.W., Sudhof, T.C., and Wernig, M. (2014). Generation of induced neuronal cells by the single reprogramming factor ASCL1. Stem Cell Reports *3*, 282–296.

Congdon, E.E., Wu, J.W., Myeku, N., Figueroa, Y.H., Herman, M., Marinec, P.S., Gestwicki, J.E., Dickey, C.A., Yu, W.H., and Duff, K.E. (2012). Methylthioninium chloride (methylene blue) induces autophagy and attenuates tauopathy in vitro and in vivo. Autophagy *8*, 609–622.

D'Aiuto, L., Zhi, Y., Kumar Das, D., Wilcox, M.R., Johnson, J.W., McClain, L., MacDonald, M.L., Di Maio, R., Schurdak, M.E., Piazza, P., et al. (2014). Large-scale generation of human iPSC-derived neural stem cells/early neural progenitor cells and their neuronal differentiation. Organogenesis *10*, 365–377.

Dehdashti, S.J., Zheng, W., Gever, J.R., Wilhelm, R., Nguyen, D.T., Sittampalam, G., McKew, J.C., Austin, C.P., and Prusiner, S.B. (2013). A high-throughput screening assay for determining cellular levels of total tau protein. Curr. Alzheimer Res. *10*, 679–687.

DeVos, S.L., Goncharoff, D.K., Chen, G., Kebodeaux, C.S., Yamada, K., Stewart, F.R., Schuler, D.R., Maloney, S.E., Wozniak, D.F., Rigo, F., et al. (2013). Antisense reduction of tau in adult mice protects against seizures. J. Neurosci. *33*, 12887–12897.

Dickey, C.A., Ash, P., Klosak, N., Lee, W.C., Petrucelli, L., Hutton, M., and Eckman, C.B. (2006). Pharmacologic reductions of total tau levels; implications for the role of microtubule dynamics in regulating tau expression. Mol. Neurodegener. *1*, 6.

Fatokun, A.A., Liu, J.O., Dawson, V.L., and Dawson, T.M. (2013). Identification through high-throughput screening of 4′-methoxyflavone and 3′,4′-dimethoxyflavone as novel neuroprotective inhibitors of parthanatos. Br. J. Pharmacol. *169*, 1263–1278.

Frohman, E.M., Vayuvegula, B., Gupta, S., and van den Noort, S. (1988). Norepinephrine inhibits gamma-interferon-induced major histocompatibility class II (Ia) antigen expression on cultured astrocytes via beta-2-adrenergic signal transduction mechanisms. Proc. Natl. Acad. Sci. USA *85*, 1292–1296.

Gruninger, F. (2015). Invited review: drug development for tauopathies. Neuropathol. Appl. Neurobiol. *41*, 81–96.

K Hancock, M., Kopp, L., Kaur, N., and Hanson, B.J. (2015). A facile method for simultaneously measuring neuronal cell viability and neurite outgrowth. Curr. Chem. Genom. Transl. Med. *9*, 6–16.

Harrill, J.A., Robinette, B.L., Freudenrich, T., and Mundy, W.R. (2013). Use of high content image analyses to detect chemical-mediated effects on neurite sub-populations in primary rat cortical neurons. Neurotoxicology *34*, 61–73.

Hester, M.E., Murtha, M.J., Song, S., Rao, M., Miranda, C.J., Meyer, K., Tian, J.B., Boulting, G., Schaffer, D.V., Zhu, M.X., et al. (2011). Rapid and efficient generation of functional motor neurons from human pluripotent stem cells using gene delivered transcription factor codes. Mol. Ther. *19*, 1905–1912.

Hosokawa, M., Arai, T., Masuda-Suzukake, M., Nonaka, T., Yamashita, M., Akiyama, H., and Hasegawa, M. (2012). Methylene blue reduced abnormal tau accumulation in P301L tau transgenic mice. PLoS One *7*, e52389.

Ittner, L.M., Ke, Y.D., Delerue, F., Bi, M., Gladbach, A., van Eersel, J., Wolfing, H., Chieng, B.C., Christie, M.J., Napier, I.A., et al. (2010). Dendritic function of tau mediates amyloid-beta toxicity in Alzheimer's disease mouse models. Cell *142*, 387–397.

Jain, S., van Kesteren, R.E., and Heutink, P. (2012). High content screening in neurodegenerative diseases. J. Vis. Exp., e3452.

Kordeli, E., Lambert, S., and Bennett, V. (1995). AnkyrinG. A new ankyrin gene with neural-specific isoforms localized at the axonal initial segment and node of Ranvier. J. Biol. Chem. *270*, 2352–2359.

Lasagna-Reeves, C.A., de Haro, M., Hao, S., Park, J., Rousseaux, M.W., Al-Ramahi, I., Jafar-Nejad, P., Vilanova-Velez, L., See, L., De Maio, A., et al. (2016). Reduction of Nuak1 decreases tau and reverses phenotypes in a tauopathy mouse model. Neuron *92*, 407–418.

Li, S., Jin, M., Zhang, D., Yang, T., Koeglsperger, T., Fu, H., and Selkoe, D.J. (2013). Environmental novelty activates beta2-adrenergic signaling to prevent the impairment of hippocampal LTP by Abeta oligomers. Neuron *77*, 929–941.

Di Maria, E., Tabaton, M., Vigo, T., Abbruzzese, G., Bellone, E., Donati, C., Frasson, E., Marchese, R., Montagna, P., Munoz, D.G., et al. (2000). Corticobasal degeneration shares a common genetic background with progressive supranuclear palsy. Ann. Neurol. *47*, 374–377.

Mather, M., and Harley, C.W. (2016). The locus coeruleus: essential for maintaining cognitive function and the aging brain. Trends Cogn. Sci. *20*, 214–226.

Medda, X., Mertens, L., Versweyveld, S., Diels, A., Barnham, L., Bretteville, A., Buist, A., Verheyen, A., Royaux, I., Ebneth, A., et al. (2016). Development of a scalable, high-throughput-compatible assay to detect Tau aggregates using iPSC-derived cortical neurons maintained in a three-dimensional culture format. J. Biomol. Screen. *21*, 804–815.

Meredith, J.E., Jr., Sankaranarayanan, S., Guss, V., Lanzetti, A.J., Berisha, F., Neely, R.J., Slemmon, J.R., Portelius, E., Zetterberg, H., Blennow, K., et al. (2013). Characterization of novel CSF Tau and ptau biomarkers for Alzheimer's disease. PLoS One *8*, e76523.

Min, S.W., Chen, X., Tracy, T.E., Li, Y., Zhou, Y., Wang, C., Shirakawa, K., Minami, S.S., Defensor, E., Mok, S.A., et al. (2015). Critical role of acetylation in tau-mediated neurodegeneration and cognitive deficits. Nat. Med. *21*, 1154–1162.

Miyaoka, Y., Chan, A.H., Judge, L.M., Yoo, J., Huang, M., Nguyen, T.D., Lizarraga, P.P., So, P.L., and Conklin, B.R. (2014). Isolation of single-base genome-edited human iPS cells without antibiotic selection. Nat. Methods *11*, 291–293.

Morris, M., Hamto, P., Adame, A., Devidze, N., Masliah, E., and Mucke, L. (2013). Age-appropriate cognition and subtle dopamine-independent motor deficits in aged tau knockout mice. Neurobiol. Aging *34*, 1523–1529.

Muratore, C.R., Srikanth, P., Callahan, D.G., and Young-Pearse, T.L. (2014). Comparison and optimization of hiPSC forebrain cortical differentiation protocols. PLoS One *9*, e105807.

Myers, A.J., Kaleem, M., Marlowe, L., Pittman, A.M., Lees, A.J., Fung, H.C., Duckworth, J., Leung, D., Gibson, A., Morris, C.M., et al. (2005). The H1c haplotype at the MAPT locus is associated with Alzheimer's disease. Hum. Mol. Genet. *14*, 2399–2404.

Myers, A.J., Pittman, A.M., Zhao, A.S., Rohrer, K., Kaleem, M., Marlowe, L., Lees, A., Leung, D., McKeith, I.G., Perry, R.H., et al. (2007). The MAPT H1c risk haplotype is associated with increased expression of tau and especially of 4 repeat containing transcripts. Neurobiol. Dis. *25*, 561–570.

Nelson, P.T., Alafuzoff, I., Bigio, E.H., Bouras, C., Braak, H., Cairns, N.J., Castellani, R.J., Crain, B.J., Davies, P., Del Tredici, K., et al. (2012). Correlation of Alzheimer disease neuropathologic changes with cognitive status: a review of the literature. J. Neuropathol. Exp. Neurol. *71*, 362–381.

Ni, Y., Zhao, X., Bao, G., Zou, L., Teng, L., Wang, Z., Song, M., Xiong, J., Bai, Y., and Pei, G. (2006). Activation of beta2-adrenergic receptor stimulates gamma-secretase activity and accelerates amyloid plaque formation. Nat. Med. *12*, 1390–1396.

Nicholas, C.R., Chen, J., Tang, Y., Southwell, D.G., Chalmers, N., Vogt, D., Arnold, C.M., Chen, Y.J., Stanley, E.G., Elefanty, A.G., et al. (2013). Functional maturation of hPSC-derived forebrain interneurons requires an extended timeline and mimics human neural development. Cell Stem Cell *12*, 573–586.

Pang, Z.P., Yang, N., Vierbuchen, T., Ostermeier, A., Fuentes, D.R., Yang, T.Q., Citri, A., Sebastiano, V., Marro, S., Sudhof, T.C., et al. (2011). Induction of human neuronal cells by defined transcription factors. Nature *476*, 220–223.

Panza, F., Solfrizzi, V., Seripa, D., Imbimbo, B.P., Lozupone, M., Santamato, A., Tortelli, R., Galizia, I., Prete, C., Daniele, A., et al. (2016). Tau-based therapeutics for Alzheimer's disease: active and passive immunotherapy. Immunotherapy *8*, 1119–1134.

Pascual, J., Grijalba, B., Garcia-Sevilla, J.A., Zarranz, J.J., and Pazos, A. (1992). Loss of high-affinity alpha 2-adrenoceptors in Alzheimer's disease: an autoradiographic study in frontal cortex and hippocampus. Neurosci. Lett. *142*, 36–40.

Roberson, E.D., Scearce-Levie, K., Palop, J.J., Yan, F., Cheng, I.H., Wu, T., Gerstein, H., Yu, G.Q., and Mucke, L. (2007). Reducing endogenous tau ameliorates amyloid beta-induced deficits in an Alzheimer's disease mouse model. Science *316*, 750–754.

Roberson, E.D., Halabisky, B., Yoo, J.W., Yao, J., Chin, J., Yan, F., Wu, T., Hamto, P., Devidze, N., Yu, G.Q., et al. (2011). Amyloid-beta/Fyn-induced synaptic, network, and cognitive impairments depend on tau levels in multiple mouse models of Alzheimer's disease. J. Neurosci. *31*, 700–711.

Santacruz, K., Lewis, J., Spires, T., Paulson, J., Kotilinek, L., Ingelsson, M., Guimaraes, A., DeTure, M., Ramsden, M., McGowan, E., et al. (2005). Tau suppression in a neurodegenerative mouse model improves memory function. Science *309*, 476–481.

Schlachetzki, J.C., Fiebich, B.L., Haake, E., de Oliveira, A.C., Candelario-Jalil, E., Heneka, M.T., and Hull, M. (2010). Norepinephrine enhances the LPS-induced expression of COX-2 and secretion of PGE2 in primary rat microglia. J. Neuroinflammation *7*, 2.

Soeda, Y., Yoshikawa, M., Almeida, O.F., Sumioka, A., Maeda, S., Osada, H., Kondoh, Y., Saito, A., Miyasaka, T., Kimura, T., et al. (2015). Toxic tau oligomer formation blocked by capping of cysteine residues with 1,2-dihydroxybenzene groups. Nat. Commun. *6*, 10216.

Spires-Jones, T.L., Kopeikina, K.J., Koffie, R.M., de Calignon, A., and Hyman, B.T. (2011). Are tangles as toxic as they look? J. Mol. Neurosci. *45*, 438–444.

Spittaels, K., Van den Haute, C., Van Dorpe, J., Bruynseels, K., Vandezande, K., Laenen, I., Geerts, H., Mercken, M., Sciot, R., Van Lommel, A., et al. (1999). Prominent axonopathy in the brain and spinal cord of transgenic mice overexpressing four-repeat human tau protein. Am. J. Pathol. *155*, 2153–2165.

Sydow, A., Van der Jeugd, A., Zheng, F., Ahmed, T., Balschun, D., Petrova, O., Drexler, D., Zhou, L., Rune, G., Mandelkow, E., et al. (2011). Tau-induced defects in synaptic plasticity, learning, and memory are reversible in transgenic mice after switching off the toxic Tau mutant. J. Neurosci. *31*, 2511–2525.

Szabo, C., Hasko, G., Zingarelli, B., Nemeth, Z.H., Salzman, A.L., Kvetan, V., Pastores, S.M., and Vizi, E.S. (1997). Isoproterenol regulates tumour necrosis factor, interleukin-10, interleukin-6 and nitric oxide production and protects against the development of vascular hyporeactivity in endotoxaemia. Immunology *90*, 95–100.

Uberti, D., Rizzini, C., Spano, P.F., and Memo, M. (1997). Characterization of tau proteins in human neuroblastoma SH-SY5Y cell line. Neurosci. Lett. *235*, 149–153.

Vossel, K.A., Zhang, K., Brodbeck, J., Daub, A.C., Sharma, P., Finkbeiner, S., Cui, B., and Mucke, L. (2010). Tau reduction prevents Abeta-induced defects in axonal transport. Science *330*, 198.

Wang, Y., and Mandelkow, E. (2016). Tau in physiology and pathology. Nat. Rev. Neurosci. *17*, 5–21.

Wisely, E.V., Xiang, Y.K., and Oddo, S. (2014). Genetic suppression of beta2-adrenergic receptors ameliorates tau pathology in a mouse model of tauopathies. Hum. Mol. Genet. *23*, 4024–4034.

Wittmann, C.W., Wszolek, M.F., Shulman, J.M., Salvaterra, P.M., Lewis, J., Hutton, M., and Feany, M.B. (2001). Tauopathy in *Drosophila*: neurodegeneration without neurofibrillary tangles. Science *293*, 711–714.

Yu, J.T., Tan, L., Ou, J.R., Zhu, J.X., Liu, K., Song, J.H., and Sun, Y.P. (2008). Polymorphisms at the beta2-adrenergic receptor gene influence Alzheimer's disease susceptibility. Brain Res. *1210*, 216–222.

Zhang, J.H., Chung, T.D.Y., and Oldenburg, K.R. (1999). A simple statistical parameter for use in evaluation and validation of high throughput screening assays. J. Biomol. Screen. *4*, 67–73.

Zhang, X.D., Yang, X.C., Chung, N., Gates, A., Stec, E., Kunapuli, P., Holder, D.J., Ferrer, M., and Espeseth, A.S. (2006). Robust statistical methods for hit selection in RNA interference high-throughput screening experiments. Pharmacogenomics *7*, 299–309.

Zhang, Y., Pak, C., Han, Y., Ahlenius, H., Zhang, Z., Chanda, S., Marro, S., Patzke, C., Acuna, C., Covy, J., et al. (2013). Rapid single-step induction of functional neurons from human pluripotent stem cells. Neuron *78*, 785–798.

Stem Cell Reports, Volume *9*

Supplemental Information

Scalable Production of iPSC-Derived Human Neurons to Identify Tau-Lowering Compounds by High-Content Screening

Chao Wang, Michael E. Ward, Robert Chen, Kai Liu, Tara E. Tracy, Xu Chen, Min Xie, Peter Dongmin Sohn, Connor Ludwig, Anke Meyer-Franke, Celeste M. Karch, Sheng Ding, and Li Gan

Supplemental Figures and Legends

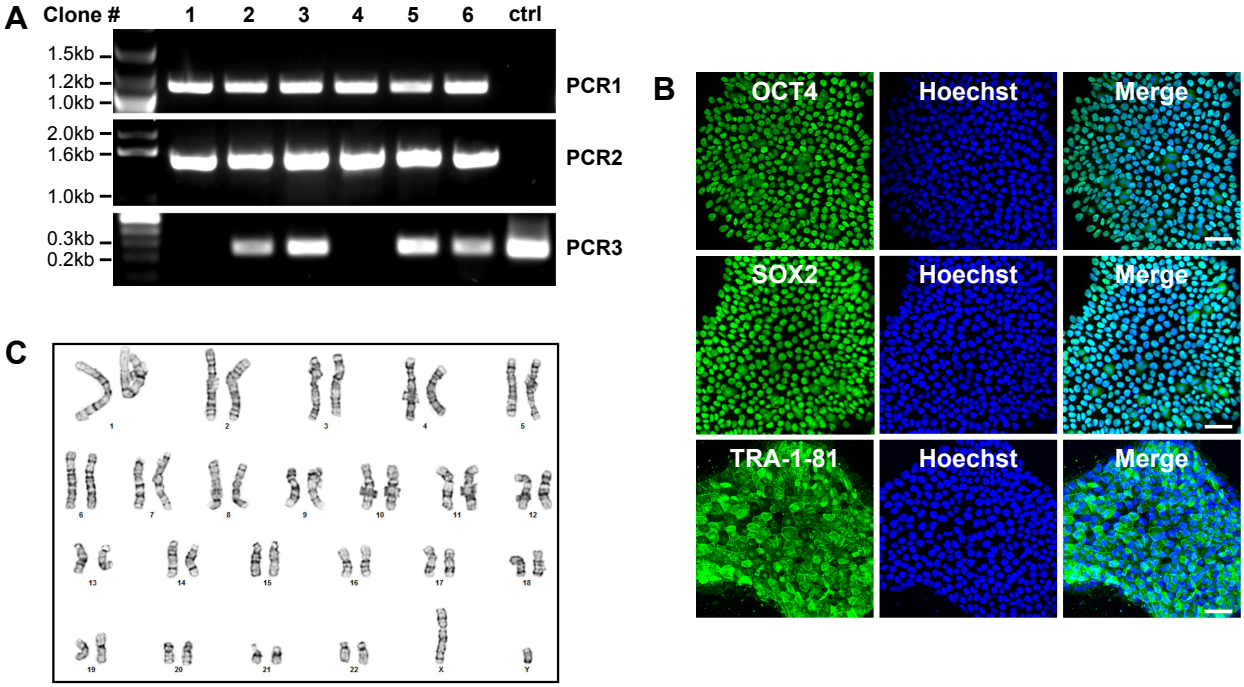

Figure S1. Characterization of i3N iPSC line. Related to Figure 1
(A) PCR1-3 results of six puromycin-resistant clones. The original WTC11 iPSC line served as control (ctrl).
(B) Representative images showing immunostaining of i^{3}N iPSC clone 1 for the pluripotency markers OCT4,SOX2, and TRA-1-81. Nuclei were labeled by Hoechst. Scale bar, 50 μm
(C) G-banded karyotype analysis of i^{3}N iPSC clone 1

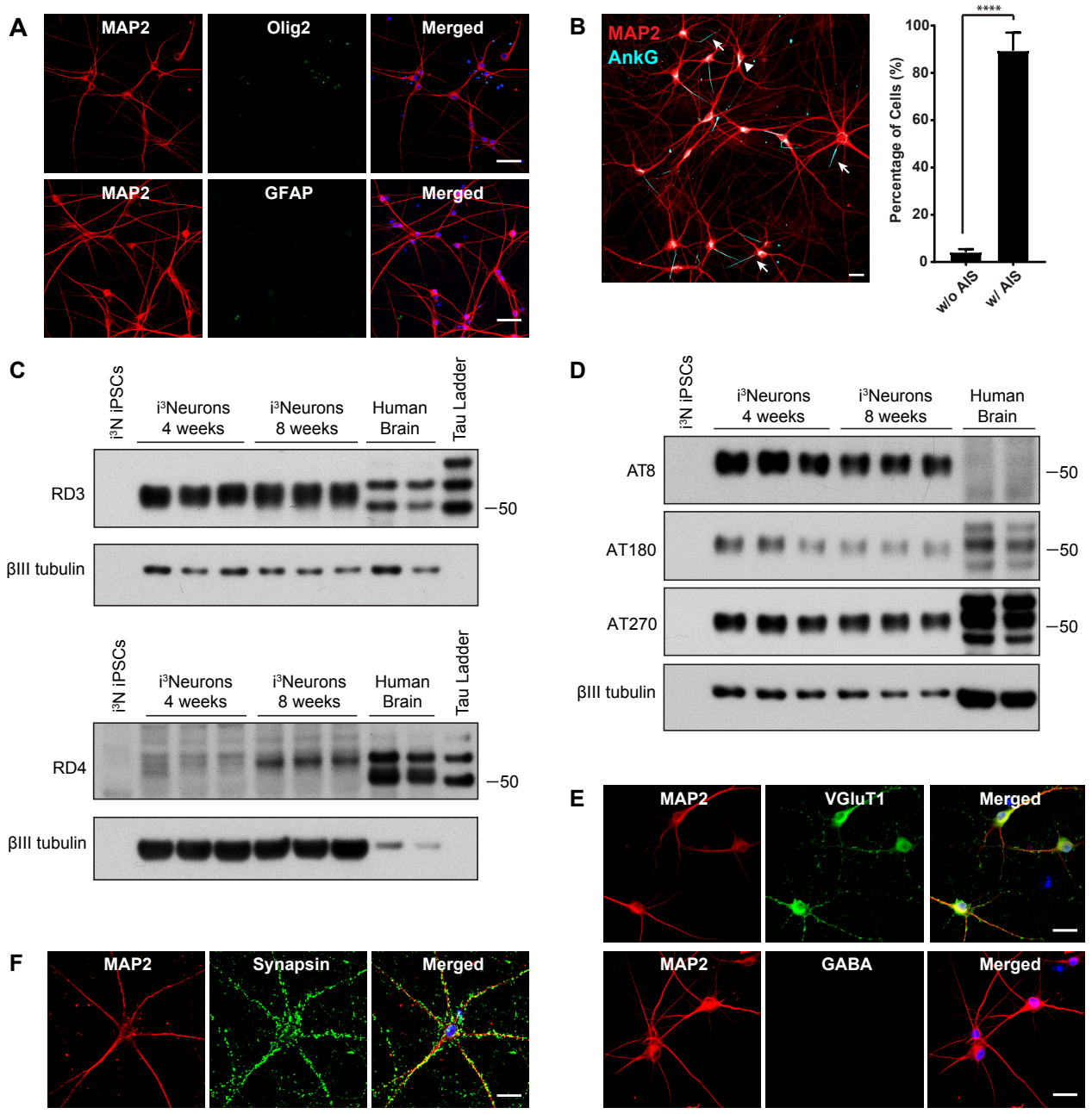

Figure S2. Characterization of i³Neurons. Related to Figure 1

(A) Representative images of immunocytochemical staining show no expression of the oligodendrocyte maker Olig2 or the astrocyte marker GFAP in mature 8-week-old i³Neurons. Nuclei were labeled by Hoechst. Scale bar, 50 μm.

(B) Representative image of immunocytochemical staining of AIS marker AnkG and dendritic marker MAP2 (left) and quantification of i³Neurons with or without AIS (right). Arrow, i³Neuron with AIS; arrowhead, i³Neuron without AIS. Scale bar, 20 μm. Values are means ± SEM. Data are from three independent culture, total N=331 neurons. ****p<0.0001, two-tailed unpaired student t-test.

(C) Western blot analysis of 3R tau isoforms (RD3) and 4R tau isoforms (RD4) in i³N iPSCs and 4- and 8-week i³Neurons and healthy human brain. Neuron loading is determined by βIII tubulin.

(D) Western blot analysis of tau phosphorylation at Ser202/Thr205 (AT8), Thr231 (AT180) and Thr181 (AT270) in i³N iPSCs and 4- and 8-week i³Neurons and healthy human brain. Neuron loading is determined by βIII tubulin.

(E) Representative images of immunocytochemical staining show uniform expression of the glutamatergic neuronal marker vGlut1 and absence of GABA-positive inhibitory neurons in i³Neurons after 4 weeks of differentiation. Nuclei were labeled by Hoechst. Scale bar, 25 μm

(F) Representative images of immunocytochemical staining for the pre-synaptic marker synapsin-1 in mature 8-week-old i³Neurons. Nuclei were labeled by Hoechst. Scale bar, 25 μm

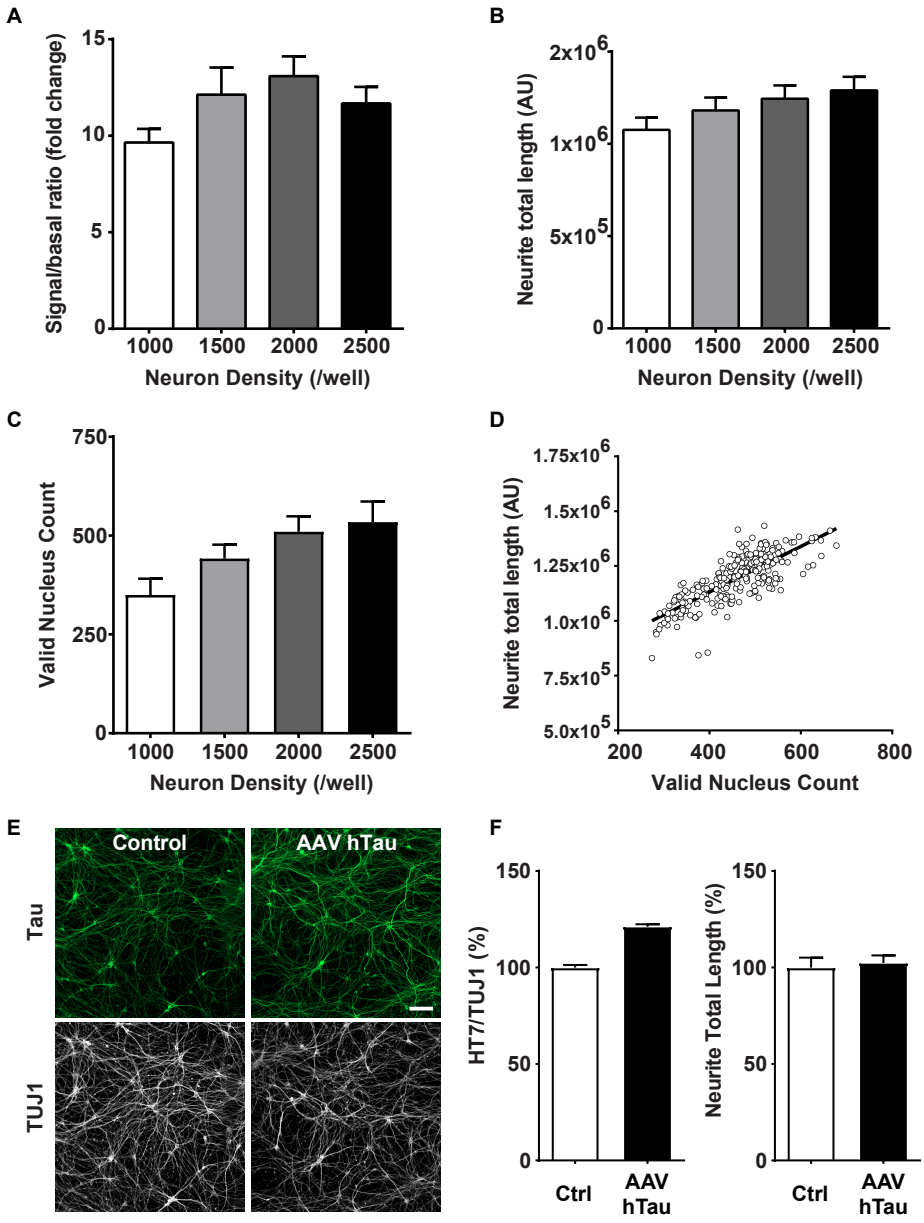

Figure S3. Optimization and validation of the tau HCS assay. Related to Figure 3

(A-D) Optimizing i^{3}Neuron density for HCS assay. Signal-to-background ratio **(A)**, neurite total length **(B)** and valid nucleus count **(C)** of high-content total tau assay were determined at seeding densities of 1000, 1500, 2000, and 2500 cells/well in 384-well plates. The signal-to-background ratio was calculated according to automated quantification of human tau signal (normalized to the TUJ1 signal) from control wells and background wells as described in Figure 3B. **(D)** Neurite total length is highly correlated with valid nucleus number. Pearson r=0.78. Results are from one experiment. For each density, N= 32 control wells and 32 background wells. Values are means ± SEM. AU: artificial unit.

(E,F) Increased human tau levels were detected by HCS assay. Representative high-content images of tau and βIII tubulin **(E)** and automated quantification of tau levels and neurite total length **(F)** from i^{3}Neurons infected with AAV full-length human tau. Scale bar, 100 μm. Results are from one experiment, N=16 control wells and AAV htau wells, values are means ± SEM. relative to control.

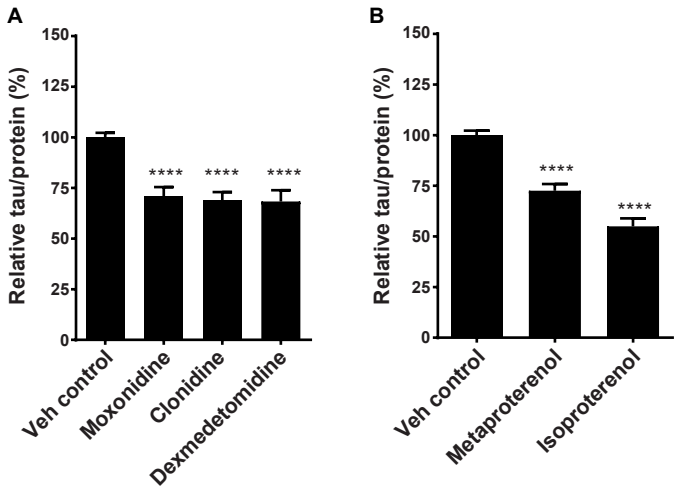

Figure S4 Activation of α- and β-AR reduces endogenous tau levels in i^{3}Neurons derived from independent i^{3}N iPSC line. Related to Figure 5

An independent iPSC line (F12486.13) was engineered to i^{3}N iPSC line at AAVS1 locus and differentiated to i^{3}Neurons using techniques described in Figure 1. 3-day incubation with α-AR agonists moxonidine (30 μM), clonidine (100 μM) and dexmedetomidine (100 μM) **(A)** or β-AR agonists metaproterenol (30 μM) and isoproterenol (30 μM) **(B)** significantly reduced endogenous tau levels in i^{3}Neurons. Human tau levels were quantified by HT7-Tau5 ELISA and normalized to protein level. Values are means ± SEM. relative to vehicle control. Data are from three independent experiments performed in triplicate, N=9 per treatment. ****P < 0.0001, STATA mixed model

Supplemental Table

Table S1. Real-time qPCR primers list. Related Figure 2

Gene Name	Description	Forward	Reverse
ANK2	adaptor protein, VGSC initiation zone	AGC ACT CTT TCC CCA AAC TC	TCT CTG ATG TTT CTG TTC CTG G
TUBB3	pan-neuronal	TTT GGA CAT CTC TTC AGG CC	TTT CAC ACT CCT TCC GCA C
MAP2	pan-neuronal	CAG GAG ACA GAG ATG AGA ATT CC	CAG GAG TGA TGG CAG TAG AC
NCAM1	pan-neuronal	GAC ATC ACC TGC TAC TTC CTG	GGC TCC TTG GAC TCA TCT TTC
DCX	pan-neuronal	TCA GGG AGT GCG TTA CAT TTA C	GTT GGG ATT GAC ATT CTT GGT G
RBFOX3	pan-neuronal	GTA GAG GGA CGG AAA ATT GAG G	CAT AGA ATT CAG GCC CGT AGA C
ELAVL1	pan-neuronal	AGA CGC CAA CTT GTA CAT CAG	ATA AAC GCA ACC CCT CTG G
GLUR1/GRIA1	AMPA receptors	TGA TGG AAA ATA CGG AGC CC	CTT CCC GGA CCA AAG TGA TAG
GLUR2/GRIA2	AMPA receptors	TCT CTG GTT TTC CTT GGG TG	CAG TCA GGA AGG CAG CTA AG
GRIA3	AMPA receptors	GTC TTT GGT TTT CCT TGG GTG	CAG CGA GAT TGG CAG TAT AGG
GRIA4	AMPA receptors	CAA GGA GAG GAA ATG CTG GG	ACG TCC ATA GTG GTC AAA CTG
NR1/GRIN1	NMDA receptors	GAG AAG GAG AAC ATC ACC GAC	GTC CCC ATC CTC ATT GAA CTC
NR2A/GRIN2A	NMDA receptors	CGC TGT CAT ATT CCT GGC TAG	GCA CTG TCC CAA ATC GAA AAG
NR2B/GRIN2B	NMDA receptors	CGT GGC TGT CTT TGT CTT TG	ACC CCA GAG CAA CCA AAT AG
VGLUT1/SLC17A7	glutamate related, glutamate transport	TCA ATA ACA GCA CGA CCC AC	TCC TGG AAT CTG AGT GAC AAT G
VGLUT2/SLC17A6	glutamate related, glutamate transport	TGG TCG TTG GCT ATT CTC ATA C	ATA CTG GCA TAT CTT GGA GCG
CAMK2A	glutamate related, glutamate transport	CAG TTC CAG CGT TCA GTT AAT G	TTC GTG TAG GAC TCA AAA TCT CC
GABRA2	GABA Receptor	TTA GCC AGC ACC AAC CTG	TCG TCA AGA TCA GGG CAA AAG
GABRB1	GABA Receptor	TGC TGG AAA TAC ATG GTG AGT G	AGT GGA CAG ATT GCT CAA AGG
GAD65/GAD2	GABA Synthesis	CAC CAT CTC ATA TCC TTC TCG G	AAA CTA TGG CTG ATG TGG AGG
GAD67/GAD1	GABA Synthesis	CAC TCA CAA GGC GAC TCT TC	GAC CCC AAT ACC ACT AAC CTG
VGAT/SLC32A1	GABA Transporter	AGA TGA TGA GAA ACA ACC CCA G	CAC GAC AAG CCC AAA ATC AC
SYN1	pre-synaptic	CCC CAA TCA CAA AGA AAT GCT C	ATG TCC TGG AAG TCA TGC TG
PSD95/DLG4	post-synaptic	AGT CAG AAA TAC CGC TAC CAA G	CCG TTC ACC TGC AAC TCA TAT C
SHANK3	post-synaptic	ATC AAG ACC CAC AAA GAC TCG	CCC TTC AGG TTG ATA TCG CTG
KCNC1	potassium channel,Kv3 type/shaw related fast spiking	TCT TCG AGG ACC CGT ACT C	CTC GAT CTC CGT CTT GTT CAC

KCNC3	potassium channel,Kv3 type/shaw related fast spiking	GAC AAG AGC CCC ATC ACG	GCT TAC GCC AGT CTT GGG
RELN	telencephalic	TCT ACC TTC CAC TCT CCA CC	ATC ACA AAT CCC TCG TCC TG
SOX5	telencephalic	TCA TGG TGT GGG CTA AAG ATG	TGG CTG TTT CTC TAG GTT TGT C
BRN2/POU3F2	telencephalic	AAA GTA ACT GTC AAA TGC GCG	GCT GTA GTG GTT AGA CGC TG
OTX2	telencephalic	CCA GAC ATC TTC ATG CGA GAG	GGC AGG TCT CAC TTT GTT TTG
LHX2	telencephalic	GGT CTT CCC TAC TAC AAT GGC	GTC GTT TTC GTT GCA GCT TAG
ROR-BETA/RORB	telencephalic	GCA GAC CCA CAC CTA TGA AG	TCC ATG AAG CCT GTT ATC CG
TBR1	telencephalic	GGA GCT TCA AAT AAC AAT GGG C	GAG TCT CAG GGA AAG TGA ACG
CUX1	cortical(layer 2/3)	TCA CCT CTT CAT AGT CAG CCT	CAG CCA GAT CTC ACA GCT TG
SATB2	cortical	CCT TAC GCA GAA TCT CAG ACA A	CCA GAT ATC TAC CAG CAA GTC AG
CTGF	cortical	GCT CGG TAT GTC TTC ATG CTG	GAA GCT GAC CTG GAA GAG AAC
TLE4	cortical	GAT GAG GAT TCT TTG GAC TGG A	GTG CTG TCG CTC AAG TTT G
CTIP2/BCL11B	cortical	GTT GTG CAA ATG TAG CTG GAA	GAA GAT GAC CAC CTG CTC TC
CLIM1/LDB2	cortical	ACT TCT GAA ACA AGC AGG TCT	CAA ACT TCA CCC TCA ACT ACC T
NR2F1	cortical	AGA TGT AGC CGG ACA GGT AG	CTC AAG AAG TGC CTC AAA GTG
BHLHB5/BHLHE22	cortical	CAT ACT CCA TCC CAA CTC CAC	GAG GCA AGA ACT GAG GAG AAG
DIAPH3	cortical	GTA GCG TTG TTT TCT GAT CTG C	GCT GGA ACT TGT ATT GCT AAT GG
FEZF2	cortical	GTC AGC TTG TGG TTC TTG TAG T	ACG CTC AAC ACG CAT ATC C
FOG2/ZFPM2	cortical	ATG GCC TTC GTA GTT GTA CAC	TGG TTG CTG GAT GTG ACT TG
OTX1	cortical	ACC ACG CAG TCC TTC AG	GAT CCA GGT AGA TGG TGA ACG
PAX6	NPC marker	GCC CTC ACA AAC ACC TAC AG	TCA TAA CTC CGC CCA TTC AC
NESTIN/NES	NPC marker	TGC GGG CTA CTG AAA AGT TC	GGC TGA GGG ACA TCT TGA G
GFAP	Glia	GAA GCT CCA AGA TGA AAC CAA C	CCT CCA GCG ATT CAA CCT TT
OLIG2	Glia	AGA TAG TCG TCG CAG CTT TC	GTT CTC CCC TGA GGC TTT TC
MBP	Glia	TCC TCT CCC CTT TCC CTG	CCC AAG ATG AAA ACC CCG TAG
NGN2/NEUROG2	neural-specific bHLH transcription factor	TAC CTC CTC TTC CTC CTT CA	GAC ATT CCC GGA CAC ACA C
GAPDH	internal ctrl	GGC CAT CCA CAG TCT TCT G	TCA TCA GCA ATG CCT CCT G

Supplemental Experimental Procedures

Generating and selecting integrated, isogenic, and inducible neurogenin-2 (i^3N) iPSC clones. The original pUCM donor vector, which contains AAVS1 homology arms and the Tet-On 3G system, and a TALEN nuclease expression pair that targets the AAVS1 locus (kind gifts from Dr. Bruce Conklin, Gladstone Institutes) have been characterized. Hemagglutinin-tagged mouse Ngn2 (a kind gift from Dr. Thomas C. Südhof, Stanford University) was subcloned downstream of TRE3G (tet response element) in the pUCM vector (pUCM-Ngn2) with In-Fusion Cloning kits (Clontech Laboratories). A reverse tetracycline-controlled transactivator (rtTA3G, driven by the CAG promoter) and mouse Ngn2, were arranged in a tail-to-tail orientation. A splicing acceptor-linked puromycin in the pUCM vector facilitates selection of clones in which the donor plasmid is integrated at the AAVS1 locus. A well-characterized human iPSC line with a wildtype genetic background (WTC11) and another independent wildtype human iPSC line F12486.13 were used to generate Ngn2-integrated clones by a DNA-In Stem transfection reagent (MTI-GlobalStem). The iPSC lines were maintained on growth-factor reduced Matrigel (Corning) and fed every other day with Essential 8 medium (E8 medium).

The day before transfection, human iPSCs were dissociated into single cell with Accutase and plated at 1.0-1.5x10^6 cells per six-well dish in E8 medium containing the Rho-associated kinase inhibitor Y-27632 (10 μM, Cayman Chemical). For transfection, pUCM-Ngn2 donor vector (2.5 μg) and the TALEN pair (1.25 μg each) were incubated with DNA-In Stem reagent (10 μl) and OptiMEM (250 μl, Invitrogen) for 10 min and added drop-wise to iPSCs. The day after transfection, cells were dissociated with Accutase and plated at 1:6 to 1:12 on six-well dishes. Selection with puromycin (0.1–0.3 μg/ml) in E8 medium plus Y-27632 started 24–48 hours after transfection and continued for ~10 days until stable colonies formed. Parallel control transfections with donor vector but not TALEN pairs facilitated empirical determination of optimal puromycin concentrations for clonal selection. Individual colonies were picked with a P200 pipette tip under an EVOS FL microscope (Invitrogen). Genomic DNA from expanded clones was purified with DNeasy Blood & Tissue Kit (Qiagen) and genotyped with the Q5 High-Fidelity PCR system (NEB) and the following primers: PCR1 (forward: 5′-CTGCCGTCTCTCTCCTGAGT-3′; reverse: 5′-GGGCTTGTACTCGGTCATCT-3’); PCR2 (forward: 5′-GCAGCATCAGTACCTCCTCT-3′; reverse: 5′-AAAAGGCAGCCTGGTAGACA-3′); PCR3 (forward: 5′-CGGTTAATGTGGCTCTGGTT-3′; reverse: 5′-AGGATCCTCTCTGGCTCCAT-3′). Selected integrated Ngn2 clones were frozen in 90% fetal bovine serum (HyClone) and 10% DMSO. Culture medium were routinely tested for mycoplasma contamination.

Electrophysiology. i^3Neurons were submerged in external solution containing 140 mM NaCl, 5 mM KCl, 10 mM glucose, 10 mM HEPES, 2 mM $MgCl_2$, and 2.5 mM $CaCl_2$, pH 7.4. Patch pipette resistance was 3–5 MΩ. Current clamp recordings of action potentials were done with internal solution containing 135 mM K-gluconate, 10 mM HEPES, 0.1 mM EGTA, 5 mM KCl, 2 mM $MgCl_2$, 4 mM Mg-ATP, and 0.3 mM Na-GTP, pH 7.3. Picrotoxin (100 μM), CNQX (10 μM), and D-AP5 (100 μM) were added to the external solution to block synaptic inputs. The neuron was held at –60 mV, and current was injected in incremental steps of 500-ms duration. Voltage clamp recordings of excitatory postsynaptic currents were done with internal solution containing 120 mM $CsCl_2$, 10 mM HEPES, 10 mM EGTA, 5 mM NaCl, 1 mM $MgCl_2$, 4 mM Mg-ATP, 0.3 mM Na-GTP, and 10 mM QX-314, pH 7.2. AMPA receptor-mediated postsynaptic currents were blocked with CNQX (10 μM). Recordings were done with a Multiclamp 700B amplifier (Molecular Devices), digitized at 10 kHz, and acquired with WinLTP software (version 1.11b, University of Bristol).

Western Blot Analysis i^3N iPSCs and 4- and 8-week i^3Neurons and healthy human brain were homogenized and sonicated at 4 °C in N-PER™ Neuronal Protein Extraction Reagent (87792, Thermo Fisher) containing protease inhibitor cocktail and phosphatase inhibitor cocktail 2 & 3 (Sigma). Designed amounts of protein (by BCA assay) were resolved by SDS-PAGE and transferred to nitrocellulose membranes. After blocking, membranes were labeled with mouse anti-3-repeat isoform or 4-repeat isoform tau (RD3, RD4, Millipore), mouse anti-phospho-Ser202/Thr205 tau (AT8, Fisher), phospho-Thr231 tau (AT180, Fisher), phospho-Thr181 tau (AT270, Fisher), rabbit anti-βIII tubulin (ab68193, Abcam) overnight, followed by incubation with horseradish peroxidase-conjugated goat anti-rabbit IgG or goat anti-mouse IgG antibody (Millipore). Bands were visualized by enhanced chemiluminescence.

HCS assay to determine total tau levels. After pre-differentiation, i^3N precursor cells were placed in PDL pre-coated 384-well plates (781946, Greiner) at a density of 2000 cells/well in 50 μl of maturation medium. To simplify the procedure and reduce variability and staining background, no mouse glia were added. To reduce disturbance to

cells and the possibility of contamination, the medium was not changed; instead, fresh maturation medium (25 µl/well) was added with electronic multichannel pipettes on days 7 and 14. On day 18, extra medium was removed with an EL406 Washer/Dispenser (BioTek) to ensure that 50 µl of medium was left in each well. For validation of siRNA or known tau-lowering compounds, stock concentrations of human tau Accell siRNA (GE Dharmacon), salicylate, YM-01, and methylene blue (kind gifts from Dr. Jason E. Gestwicki, University of California, San Francisco) were adjusted to ensure that each well needed 5 µl of reagents to reach the desired final concentration. For HCS, 1280 compounds from LOPAC library were dissolved in DMSO at 10 mM stock concentration and distributed to three and one-half 384-well plates. Each plate contained two columns (32 wells) of DMSO controls, which were used as control wells and background wells (n = 16/each). DMSO or compounds (50 pl) were added with a BioMek FX workstation (Beckman Coulter) to reach a final concentration of 10 µM. Cells were incubated for 3 days (LOPAC), 7 days (siRNA), or 24–72 hours (salicylate, YM-01, and methylene blue) at 37 °C in 5% CO_2.

The immunostaining protocol was similar to that described in Experimental Procedures, but with two modifications: 1% bovine serum albumin (IgG-free and protease-free, Jackson ImmunoResearch) was used to reduce cost, and the permeabilization and blocking steps were combined to reduce disturbance to cells. HT7 antibody was used to detect human tau and TUJ1 antibody was used to label βIII tubulin in neurites. Nuclei were labeled with Hoechst (H3570, Invitrogen). Reagents were added with electronic multichannel pipettes, and all washing steps were done with an automated EL406 Washer/Dispenser. Images from individual wells were acquired with a fully automated ArraySan XTi high-content system (Thermo Fisher) and a 10x objective, which provides sufficient resolution to distinguish neurites. Nine fields encompassing the total well area were captured. Images were auto-quantified with the neuronal profiling module of Cellomics software (Thermo Fisher). TUJ1 immunostaining identified all of the neurites labeled with HT7 (**Figure 3B**), which was used to define the quantification area. Background of the assay was quantified in the absence of HT7 antibody (**Figure 3B**). Multiple cellular and well neuronal features were auto-quantified with Cellomics software, including valid nucleus count (quantification of viable cell number based on nuclei size and intensity), neurite total length (based on TUJ1 staining), and total tau levels (defined by HT7 intensity normalized to TUJ1 intensity).

Due to the lack of a non-toxic tau-lowering compound, Accell tau siRNA is used as positive control and control siRNA is used as negative control (N=42). Assay reproducibility and robustness is evaluated by Z'-factor calculated as follows, where μ_{c+} and σ_{c+} are the mean and standard division of positive control; μ_{c-} and σ_{c-} are the mean and standard division of negative control.

$$Z' = 1 - 3\frac{(\sigma_{c+} + \sigma_{c-})}{|\mu_{c+} - \mu_{c-}|}$$

Computed on a plate-by-plate basis, Z-score for raw value of x_i is defined as

$$Z_i = \frac{x_i - \mu_c}{\sigma_c}$$

where μ_c is the mean of all sample values on a plate and σ_c is the standard division of these values.

Human tau and βIII tubulin ELISA High-binding ELISA plates (Costar) were coated with capture antibodies (2 µg/ml) overnight at 4°C and washed with Dulbecco's phosphate-buffered saline (DPBS). Nonspecific binding was blocked with 3% bovine serum albumin (protease free, fraction V; Roche Biochemicals) (w/v) in DPBS for 2–4 hours with gentle shaking. Diluted standards or samples (50 µl) were added to each well in a final assay buffer containing 0.3% bovine serum albumin and 0.1% Tween-20 (v/v) in DPBS. After 1 h of incubation at room temperature, detection antibodies (50 µl) diluted in final assay buffer were added and incubated overnight at 4°C. The plates were washed with DPBS containing 0.05% Tween-20 and developed with alkaline phosphatase substrate. Chemiluminescence was measured with a SpectraMax M5 (Molecular Devices).

The limit of quantification was defined as the value calculated from the background signal plus three standard deviations.